Molecular Cell

Article

Purified Smc5/6 Complex Exhibits DNA Substrate Recognition and Compaction

Graphical Abstract

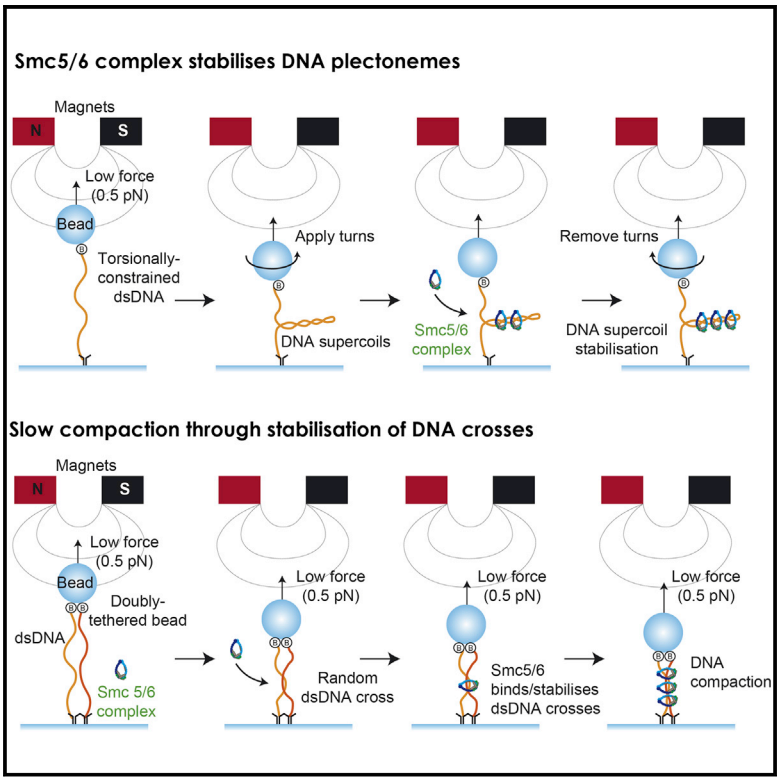

Highlights

- Purification of enzymatically active Smc5/6 yeast holocomplex
- Smc5/6 coiled-coils exhibit a folded conformation
- Smc5/6 stabilizes DNA plectonemes
- Smc5/6 compacts DNA against low forces in an ATP-dependent manner

Authors

Pilar Gutierrez-Escribano, Silvia Hormeño, Julene Madariaga-Marcos, ..., Jordi Torres-Rosell, Fernando Moreno-Herrero, Luis Aragon

Correspondence

fernando.moreno@cnb.csic.es (F.M.-H.), luis.aragon@lms.mrc.ac.uk (L.A.)

In Brief

Gutierrez-Escribano et al. purify the entire Smc5/6 holocomplex, retaining full enzymatic function. The Smc5/6 complex compacts DNA against low force and stabilizes DNA crosses present in supercoiled and catenated DNA. These findings indicate that many Smc5/6 functions occur through stabilization of DNA tertiary structure.

Gutierrez-Escribano et al., 2020, Molecular Cell *80*, 1039–1054
December 17, 2020
https://doi.org/10.1016/j.molcel.2020.11.012

CellPress

Molecular Cell

CellPress
OPEN ACCESS

Article

Purified Smc5/6 Complex Exhibits DNA Substrate Recognition and Compaction

Pilar Gutierrez-Escribano,[1,8] Silvia Hormeño,[2,8] Julene Madariaga-Marcos,[2] Roger Solé-Soler,[3] Francis J. O'Reilly,[4,5] Kyle Morris,[6] Clara Aicart-Ramos,[2] Ricardo Aramayo,[6] Alex Montoya,[7] Holger Kramer,[7] Juri Rappsilber,[4,5] Jordi Torres-Rosell,[3] Fernando Moreno-Herrero,[2,*] and Luis Aragon[1,9,*]

[1]Cell Cycle Group, MRC London Institute of Medical Sciences (LMS), Du Cane Road, London W12 0NN, UK
[2]Department of Macromolecular Structures, Centro Nacional de Biotecnología, Consejo Superior de Investigaciones Científicas, Madrid, Spain
[3]Institut de Recerca Biomèdica de Lleida (IRBLLEIDA), Department of Ciències Mèdiques Bàsiques, Universitat de Lleida, Lleida, Spain
[4]Bioanalytics, Institute of Biotechnology, Technische Universität Berlin, 13355 Berlin, Germany
[5]Wellcome Centre for Cell Biology, University of Edinburgh, Edinburgh EH9 3BF, UK
[6]Microscopy Facility, MRC London Institute of Medical Sciences (LMS), Du Cane Road, London W12 0NN, UK
[7]Biological Mass Spectrometry and Proteomics Facility, MRC London Institute of Medical Sciences (LMS), Du Cane Road, London W12 0NN, UK
[8]These authors contributed equally
[9]Lead Contact
*Correspondence: fernando.moreno@cnb.csic.es (F.M.-H.), luis.aragon@lms.mrc.ac.uk (L.A.)
https://doi.org/10.1016/j.molcel.2020.11.012

SUMMARY

Eukaryotic SMC complexes, cohesin, condensin, and Smc5/6, use ATP hydrolysis to power a plethora of functions requiring organization and restructuring of eukaryotic chromosomes in interphase and during mitosis. The Smc5/6 mechanism of action and its activity on DNA are largely unknown. Here we purified the budding yeast Smc5/6 holocomplex and characterized its core biochemical and biophysical activities. Purified Smc5/6 exhibits DNA-dependent ATP hydrolysis and SUMO E3 ligase activity. We show that Smc5/6 binds DNA topologically with affinity for supercoiled and catenated DNA templates. Employing single-molecule assays to analyze the functional and dynamic characteristics of Smc5/6 bound to DNA, we show that Smc5/6 locks DNA plectonemes and can compact DNA in an ATP-dependent manner. These results demonstrate that the Smc5/6 complex recognizes DNA tertiary structures involving juxtaposed helices and might modulate DNA topology by plectoneme stabilization and local compaction.

INTRODUCTION

Chromosome architecture and dynamics in interphase and during mitosis are controlled by structural maintenance of chromosomes (SMC) complexes (Hassler et al., 2018). Eukaryotes contain three distinct SMC complexes known as cohesin, condensin, and Smc5/6 (Jeppsson et al., 2014b). They form ring-shaped structures and use ATP hydrolysis to fuel manipulation of chromatin to change the topology of chromosomes (Hassler et al., 2018). SMC complexes invariably contain a pair of SMC proteins at their core (Losada and Hirano, 2005). SMCs are large proteins with N- and C-terminal regions separated by coiled-coil domains and a flexible hinge that allows the proteins to fold back at the middle (Hirano, 2005; Nasmyth and Haering, 2005). The N and C-terminal regions come together, generating an ATP-binding motif. SMC complexes are produced when a heterodimer of SMC proteins dimerizes through the hinges and aligns in parallel, forming a rod-shaped structure approximately 50 nm long with the two ATP-binding or "head" domains at the base (Bürmann et al., 2019). SMC heads are bridged by specific kleisin subunits, creating a tripartite structure. ATP binding and hydrolysis are thought to power conformational transitions in SMC complexes that are necessary for their function on DNA.

In addition to the SMC-kleisin core, Smc5/6 complexes contain a significant number of additional subunits, referred to as non-SMC elements (Nses). In yeast, these include Nse1, Nse2 (or Mms21), Nse3, Nse4, Nse5, and Nse6 (Sergeant et al., 2005; Zhao and Blobel, 2005). Nse4 is the Smc5/6-specific kleisin that bridges the heads of Smc5 and Smc6 (Palecek et al., 2006), whereas Nse2 is a SUMO (Small Ubiquin-like modifier) E3 ligase (Andrews et al., 2005; Potts and Yu, 2005; Zhao and Blobel, 2005) that mediates SUMOylation of Smc5/6 subunits (Bermúdez-López et al., 2015) as well as other SUMO targets (Aragón, 2018). Nse2 is docked onto the coiled-coils of Smc5 (Duan et al., 2009a), and its E3 ligase activity is stimulated by DNA (Varejão et al., 2018). Purified Smc5 and Smc6 proteins bind DNA tightly through several domains on the hinges, heads, and coiled-coil regions (Alt et al., 2017; Roy and D'Amours, 2011; Roy et al., 2011,

2015). Smc5/6 complex isolated from yeast interacts with circular DNAs in a salt-resistant manner and promotes catenation of plasmids in the presence of Top2, suggesting that it can act as an intermolecular linker (Kanno et al., 2015). Nse5 and Nse6 form a subcomplex that has been reported to interact with Smc5/6 hinges in budding yeast (Duan et al., 2009a) and Smc5/6 heads in fission yeast (Pebernard et al., 2006).

The Smc5/6 complex participates in critical chromosome transactions during DNA replication (Menolfi et al., 2015; Torres-Rosell et al., 2007) and repair (Ampatzidou et al., 2006; Bermúdez-López et al., 2016; Bonner et al., 2016; De Piccoli et al., 2006; Irmisch et al., 2009; Potts et al., 2006). Smc5/6 is required for stability of damaged replication forks (Bermúdez-López et al., 2010; Branzei et al., 2006; Irmisch et al., 2009) as well as repair of DNA double-strand breaks (DSBs) by promoting homologous recombination between sister chromatids (De Piccoli et al., 2006; Potts et al., 2006) through recruitment and SUMOylation of cohesin (McAleenan et al., 2012; Wu et al., 2012).

The function of Smc5/6 is necessary during S and G2 phases (Menolfi et al., 2015) to ensure chromosome segregation (Bermúdez-López et al., 2010; Gallego-Paez et al., 2014; Lindroos et al., 2006; Torres-Rosell et al., 2005). In G2/M, Smc5/6 colocalizes with cohesin complexes on chromosomes (Jeppsson et al., 2014a). Binding of Smc5/6 on chromosome arms is increased significantly when Top2 is inactivated during replication (Jeppsson et al., 2014a). Smc5/6 chromosomal binding upon Top2 inactivation is independent of DNA damage, suggesting that it arises as a consequence of the increased topological tension caused by Top2 absence or the presence of unresolved sister chromatid intertwines (SCIs) (Jeppsson et al., 2014a).

A recently discovered function of human Smc5/6 complexes is their role in hepatocytes as a restriction factor for hepatitis B virus (HBV) infection (Decorsière et al., 2016; Murphy et al., 2016). Transcription of viral genes from HBV episomal DNA is inhibited in the presence of the Smc5/6 complex (Decorsière et al., 2016; Murphy et al., 2016). The exact molecular mechanisms are yet to be fully elucidated; however, some evidence indicates that Smc5/6 binds to restriction factors such as PJA1, which allows the complex to recognize and bind viral episomal DNA (Xu et al., 2018). Importantly, Smc5/6 binding promotes further recruitment of DNA topoisomerases (Xu et al., 2018) to the viral genomes to restrict HBV. The SUMO ligase activity of human Nse2 has been demonstrated recently to target Top2α lysine 1520 (Deiss et al., 2019), and this modification is critical for Top2α's role in chromosome segregation (Deiss et al., 2019). It is presently unclear whether Smc5/6 SUMO activity is also required for its HBV restriction role.

Smc5/6 has been linked to a number of fundamental processes on DNA, including DNA transcription, DNA replication, DNA repair, and chromosome segregation. However, the core activity of Smc5/6 and its effect on DNA are largely unknown. Phenotypic studies where Smc5/6 function is abrogated have not been able to resolve a clear role common to all scenarios the complex affects; thus, no functional name has been assigned to this complex.

Here we isolated pure recombinant Smc5/6 holocomplexes from budding yeast and investigated their architecture and biochemical activities. We show that Smc5/6 complexes, like cohesin and condensin, exhibit a rod-shaped architecture with folded coiled-coil conformations. Purified Smc5/6 exhibits SUMO E3 ligase activity as well as the ability to bind DNA topologically in an ATP-dependent manner. Topological binding was increased in substrates harboring DNA crosses (i.e., supercoiled DNA and catenanes), and analysis of purified Smc5/6 complexes on magnetic tweezers confirmed that they can indeed lock DNA plectonemes. We also show that stabilization of DNA crosses by Smc5/6 promotes slow ATP-dependent compaction in single DNA and more efficiently when two proximal DNAs are assayed. Analysis of recombinant human Smc5/6 (Serrano et al., 2020 [this issue of *Molecular Cell*]) demonstrates that the reported activities have been conserved during evolution.

RESULTS

Purified Smc5/6 Holocomplexes Exhibit DNA-Dependent ATPase and SUMO E3 Ligase Activities

Smc5/6 is one of three SMC-kleisin complexes present in budding yeast with an essential but unclear function on replicated chromosomes (Aragón, 2018). The complex contains the two SMC proteins Smc5 and Smc6, the kleisin Nse4, and five additional Nse subunits (Sergeant et al., 2005; Zhao and Blobel, 2005). Previous studies aiming to purify the holocomplex employed tandem affinity purification of endogenous yeast complexes (Kanno et al., 2015). These approaches yielded complexes contaminated with Top1 and Top2 proteins (Kanno et al., 2015). Recently, the active five-subunit SMC complex, condensin, was purified by overexpression of its subunits from galactose (*GAL*)-inducible promoters in high-copy plasmids (St-Pierre et al., 2009; Terakawa et al., 2017). We followed the same rationale and overexpressed, in budding yeast, the 8 subunits of Smc5/6 from two high-copy plasmids. We then purified budding yeast Smc5/6 holocomplexes containing Smc5, Smc6, and Nse1-6 from exponentially growing yeast cultures (Figures 1A and 1B). Purification employed affinity chromatography with a triple StrepII (Strepavidin) tag fused to the Smc6 subunit, followed by passage through a Hi-Trap Heparin HP column. The purified complex eluted as a single peak in size-exclusion chromatography (SEC) (Figure 1A), and mass spectrometry analysis confirmed the presence of Smc5/6 octamers. Top1 or Top2 contaminants were not detected in the samples.

SMC complexes use ATP hydrolysis to fuel manipulation of DNA (Hassler et al., 2018). We therefore sought to test the ATPase activity of the purified Smc5/6 holocomplexes using an ATP/NADH-coupled assay (Figure 1C). In the absence of DNA, Smc5/6 lacked ATPase activity (Figure 1C). In contrast, Smc5/6 hydrolyzed ATP (1.2 ± 0.3 ATP/s, mean ± SD; n = 4) at a similar rate as the one observed for purified condensin (Terakawa et al., 2017) in the presence of DNA (Figure 1C).

Smc5/6 contains a SUMO E3 ligase (Andrews et al., 2005; Potts and Yu, 2005; Zhao and Blobel, 2005), Nse2, docked on the Smc5 coiled-coil (Duan et al., 2009a). Thus, we sought to investigate whether our purified Smc5/6 holocomplexes exhibit SUMO E3 ligase activity. SUMOylation occurs by a sequential enzyme cascade including E1-activating enzyme (Uba2/Aos1), E2-conjugating enzyme (Ubc9), and E3-ligase (Siz1, Siz2, and Nse2) (Hay, 2001). Detection of SUMO E3 activity *in vitro* is

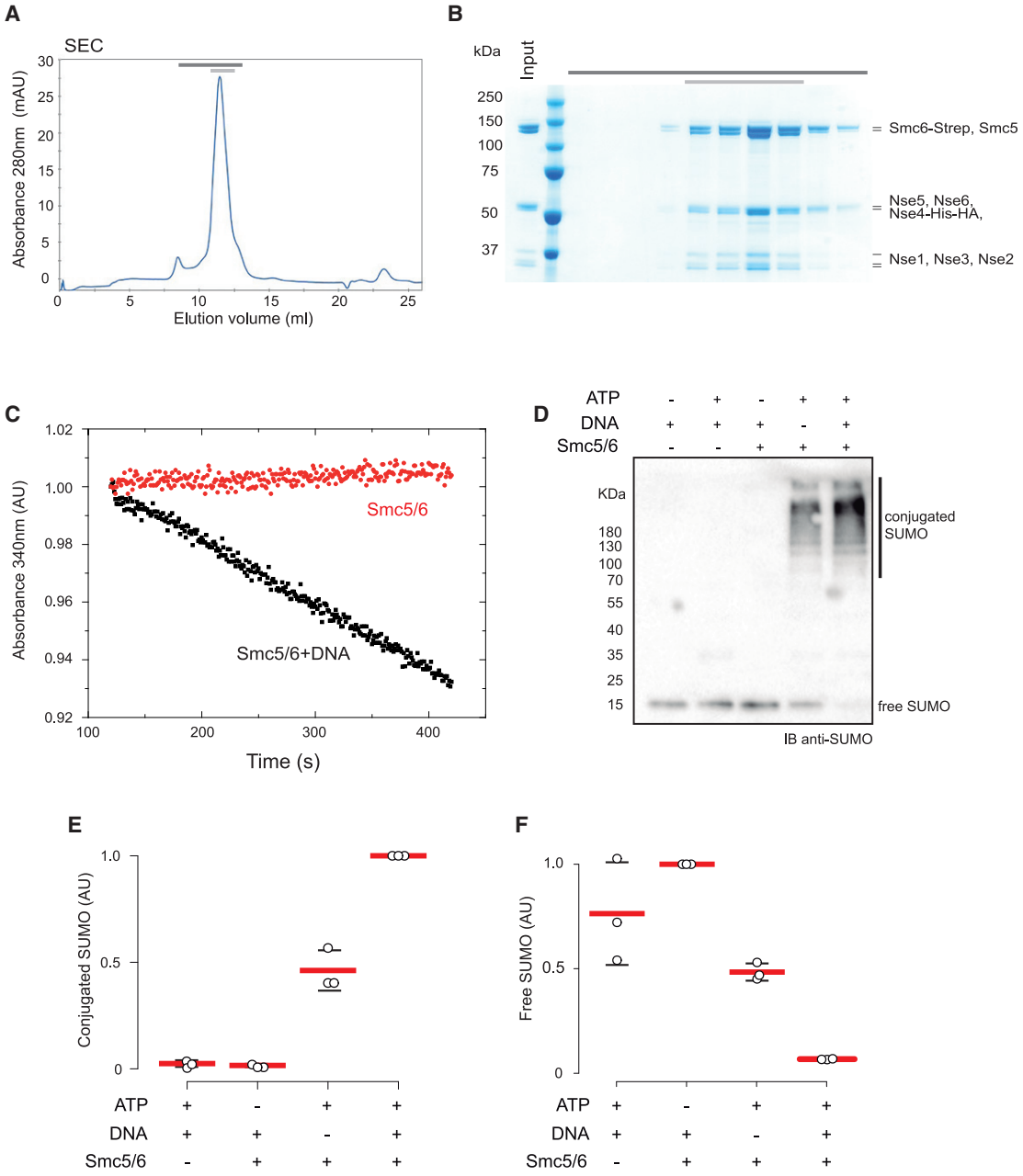

Figure 1. Purification of Budding Yeast Smc5/6 Holocomplex

(A) Size-exclusion chromatogram (SEC) of wild-type Smc5/6 complexes.

(B) Analysis of peak fractions (dark gray bar) by SDS-PAGE and Coomassie staining. The pale gray bar indicates the pooled and concentrated fractions.

(C) Representative example of an ATPase activity assay of the Smc5/6 complex in the presence and absence of relaxed circular DNA. The linear fit of the absorbance data gives the ATPase rate consumption.

(D) Anti-SUMO western blot analysis of an *in vitro* SUMOylation reaction. Reactions were started by addition of 2 mM ATP and allowed to proceed for 15 min before being stopped by addition of SDS-PAGE loading buffer. Where indicated (+), Smc5/6 and DNA were added to 165 nM and 10 nM, respectively.

(E) Quantification of conjugated bands from three independent *in vitro* SUMOylation reactions. Mean (red lines) and standard deviation (black lines) values are shown. Circles represent the individual measurements for each of the experiments.

(F) Quantification of free SUMO bands from three independent *in vitro* SUMOylation reactions. Mean (red lines) and standard deviation (black lines) values are shown. Circles represent the individual measurements for each of the experiments.

See Table S1 for further characterization of Smc5/6 purification. See Figure S1 for further characterization of Smc5/6 SUMOylation activity.

complicated because SUMO conjugation of substrates can be achieved with the E1 and E2 proteins alone, making the contribution of E3 activity difficult to detect. Smc5/6 subunits themselves are a target of Nse2 (Bermúdez-López et al., 2016); consequently, their SUMOylation status can be used as a readout of Nse2 activity. The ATPase activity of Smc5/6 and DNA binding are required for Nse2-dependent SUMOylation of Smc5 and Smc6 (Bermúdez-López et al., 2015; Varejão et al., 2018). Therefore, we carried out *in vitro* reactions using SUMO conjugation to Smc5/6 holocomplex subunits in the presence and absence of ATP and DNA (Figures 1D and 1E) to investigate whether E3 activity had been retained after purification. We followed SUMO by western blotting to quantify the amounts of conjugates present under the different conditions (Figure 1D). No conjugation was observed when Smc5/6 or ATP was omitted (Figures 1D and 1E). In the presence of Smc5/6 and ATP, SUMO conjugation was detected; however, the conjugation could be mediated solely by the presence of E1 and E2 in the reaction (Figures 1D and 1E). When DNA was also added to stimulate, the ATPase activity of Smc5/6 (Figure 1C) and its E3 SUMO ligase function (Bermúdez-López et al., 2015; Varejão et al., 2018), a significant increase in SUMO conjugation was observed (Figures 1D and 1E), and all free SUMO in the reaction was consumed (Figure 1F). In addition, we assayed Smc5/6-dependent SUMOylation of the purified C-terminal fragment of the Smc5/6 kleisin Nse4, which is a known substrate of Smc5/6 SUMO activity (Bermúdez-López et al., 2015, Varejão et al., 2018). In the absence of Smc5/6, Nse4-Ct was not SUMOylated. However, when we included Smc5/6, mono- and di-SUMOylation of Nse4-Ct were detected. These results demonstrate that Nse2 retained its E3 ligase activity in the purified Smc5/6 holocomplexes, confirming that the complexes are enzymatically active in SUMO conjugation.

EM Analysis of Purified Smc5/6

Electron microscopy (EM) images of yeast cohesin suggest that the complex adopts a rod-like structure that resembles two cherries with a stem (Bürmann et al., 2019). The coiled-coils of the Smc pair are jointed at their hinge regions, forming the stem structure; however, a discontinuity in the coiled-coils, a region called the elbow, allows the stem to fold back (Bürmann et al., 2019). The three eukaryotic SMC complexes are predicted to contain similar coiled-coil discontinuity regions that allow elbow formation in the structures (Bürmann et al., 2019). EM images of Smc5/6 complexes have not been reported to date. We crosslinked our purified Smc5/6 holocomplexes using bissulfosuccinimidyl suberate (BS^3) (Figure 2A) and analyzed their structure by negative-stain EM (Figure 2B). We observed some heterogeneity on the sample, but the particles appeared to be generally monodispersed (Figure 2B). Single particles exhibited the rod-like structure characteristic of SMC complexes (Figure 2C; Bürmann et al., 2019), with two lobbed regions at their base (Figure 2C) and stalks that varied in size emanating from them (Figure 2C). We used two-dimensional (2D) image classification to obtain class averages of the conformations (Figure 2D). The classification generated the expected two-cherries-with-a-stem structure (Figure 2D). The length of the stem was approximately 29 nm (Figure 2D), which is consistent with the bending of coiled-coils at an elbow region. We observed a similar rod-shaped organization by cryo-EM imaging (Figure 2E). The Nse2 subunit is known to interact with the coiled-coil region of Smc5 (Duan et al., 2009a; Pebernard et al., 2006). Densities on the stems of the particles were observed, which could represent Nse2 bound to Smc5 coiled-coil regions. Our EM analysis demonstrates that Smc5/6 holocomplexes present the characteristic SMC rod structure with a flexible coiled-coil region capable of bending at the elbow region.

Structural Organization of Smc5/6 Complexes

To obtain further insights into the structure of Smc5/6 complexes at the sequence level, we employed mass spectrometry to identify BS^3-crosslinked (Figure 3A) residue pairs in Smc5/6 holocomplexes. We obtained a total of 815 crosslinks at a 2% FDR (false discovery rate) (Figure 3B), of which 385 were unique inter-subunit crosslinks and 430 were intra-subunit crosslinks. Analysis of inter-subunit crosslinks between Smc5 and Smc6 confirmed the expected intimate association of these two subunits, which exhibited crosslinked pairs throughout their coiled-coil regions and heads (Figure 3C). Intra-Smc6 crosslinks revealed a domain in the hinge (around position 650) that crosslinked with the N- and C-terminal domains (Figure 3D). We also obtained crosslinked pairs between the hinge of Smc6 and the head domains of Smc5 (Figure 3C); these can only be satisfied by bending of coiled-coils, which allows the hinge region to interact with the Smc head domains (Bürmann et al., 2019). The midpoint of the interaction lies around amino acid (aa) 425 (Figure 3D), which has been predicted previously to be the elbow region based on coiled-coil discontinuities (Bürmann et al., 2019).

Previous studies had suggested that the N-terminal region of Nse2 binds to Smc5 coiled-coils (Duan et al., 2009a; Pebernard et al., 2006). We detected crosslink pairs between Nse2 and both coiled-coils of Smc5 (Figure 3E), and the Smc5 pairs mapped to the proximal and terminal regions of Nse2 (Figure 3E). In addition, crosslinks between the Nse2 N terminus and Smc6 coiled-coils were observed (Figure 3E). These results show that Nse2 sits between the two arms of the folded SMC structure. The Nse2 N-terminal region also interacts with Nse6 (Figure 3E). The number of interactions between Nse5 and Nse6 was lower than expected (Figure 3E). Nse5 and Nse6 exhibited contacts with the Smc5 and Smc6 subunits. However, Nse5 interactions were mapped to the Smc terminal head regions, whereas Nse6 crosslinked higher up on the coiled-coils (Figure 3E). Finally, Nse1, Nse3, and Nse4 crosslinks were consistent with the position of these subunits at the base of the double-cherry structure, making significant contacts with the Smc head domains (Figure 3E). We observed a significantly high number of crosslinks between Nse4 and Nse3 (Figure 3E) as well as between these two Nse subunits and the Smc5 and Smc6 heads (Figure 3E). These results indicate that Smc heads provide an interaction hub with extensive protein-protein connections to Nse4 and Nse3 subunits (Figure 3E). The crosslinking data are in good agreement with our EM analysis data demonstrating that the core of the Smc5/6 complex, formed by the SMC-kleisin, is organized in a manner similar to other Smc complexes, with the kleisin subunit Nse4 bridging the heads of Smc5 and Smc6

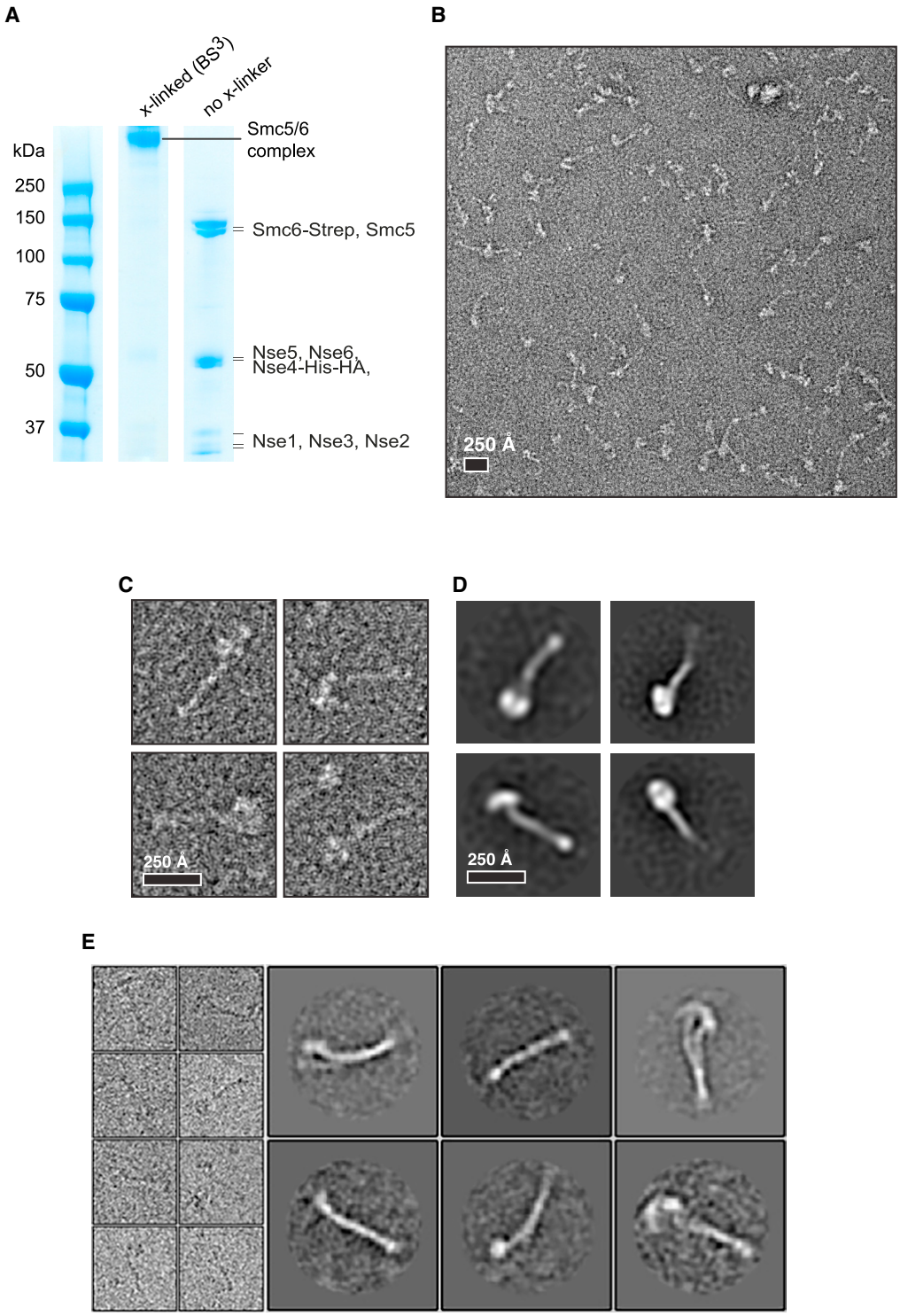

Figure 2. EM Analysis of the Purified Smc5/6 Complex

(A) SDS-PAGE of the BS^3-crosslinking stabilized complex.

(B) A typical field of view of negative-stain EM of BS^3-crosslinked Smc5/6 complex.

(C) Particle instances of the Smc5/6 complex presumed to represent the biological monomer.

(D) Negative-stain 2D class averages of (C).

(E) Cryo-EM particles (left panel) and class averages (right panel) of the Smc5/6 complex presumed to represent the biological monomer.

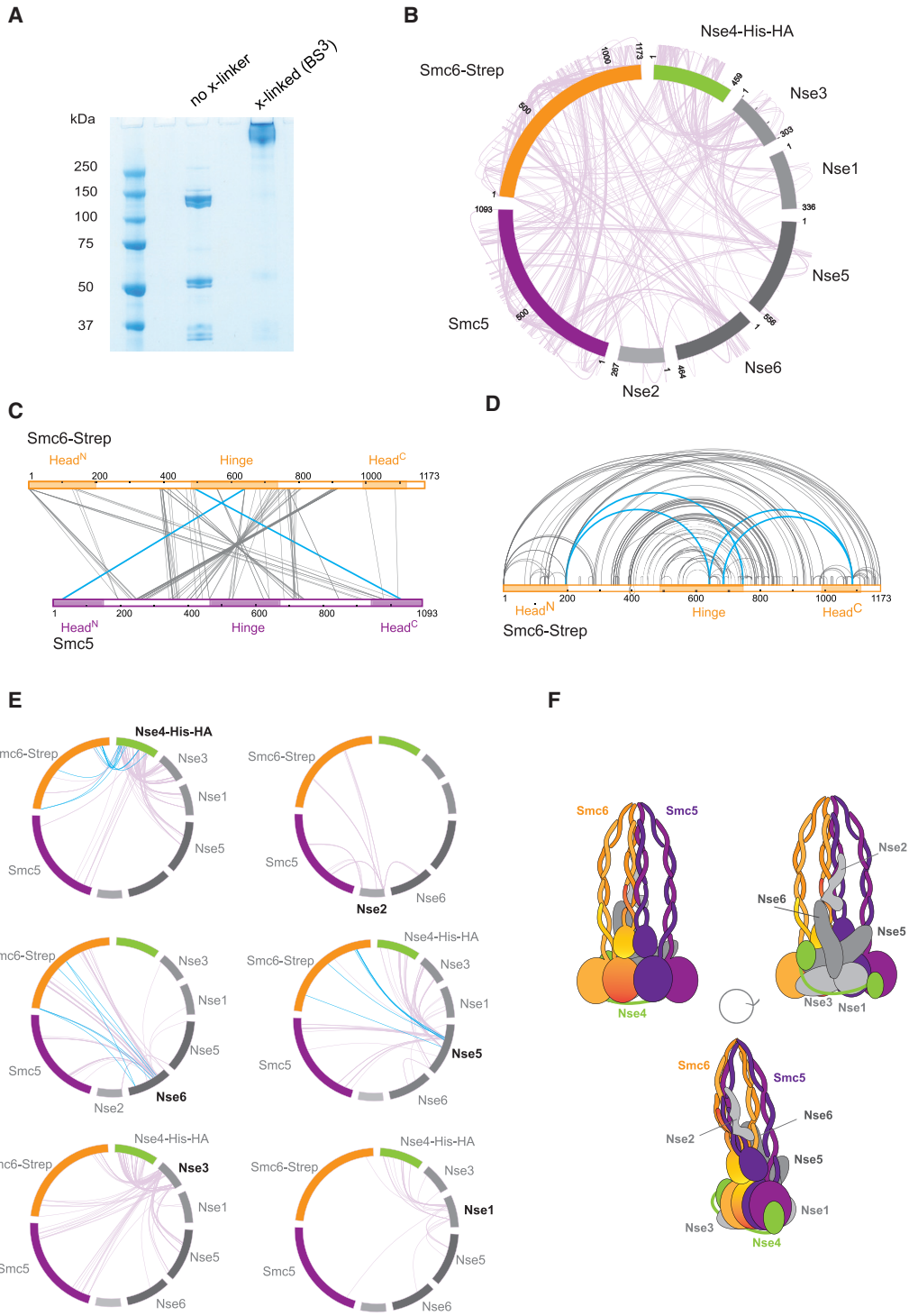

Figure 3. Crosslinking Mass Spectrometry Analysis of Smc5/6 Complex Architecture

(A) SDS-PAGE analysis of the Smc5/6 complex before and after BS^3 treatment.

(B) Intra- and inter-subunit crosslinks of the Smc5/6 complex.

(C) Inter-subunit crosslinks between Smc5 and Smc6 proteins. Head and hinge regions were annotated accordingly to Duan et al. (2009b). Throughout the whole figure, crosslinks indicating an interaction with the head and hinge regions of the Smc subunits are highlighted in blue.

(D) Smc6 intra-subunit crosslinks.

(E) Inter-subunit crosslinks of the non-SMC elements.

(F) Tentative topology of the Smc5/6 complex based on the crosslinking mass spectrometry data.

See Table S2 for further characterization of the Smc5/6 crosslinking mass spectrometry analysis.

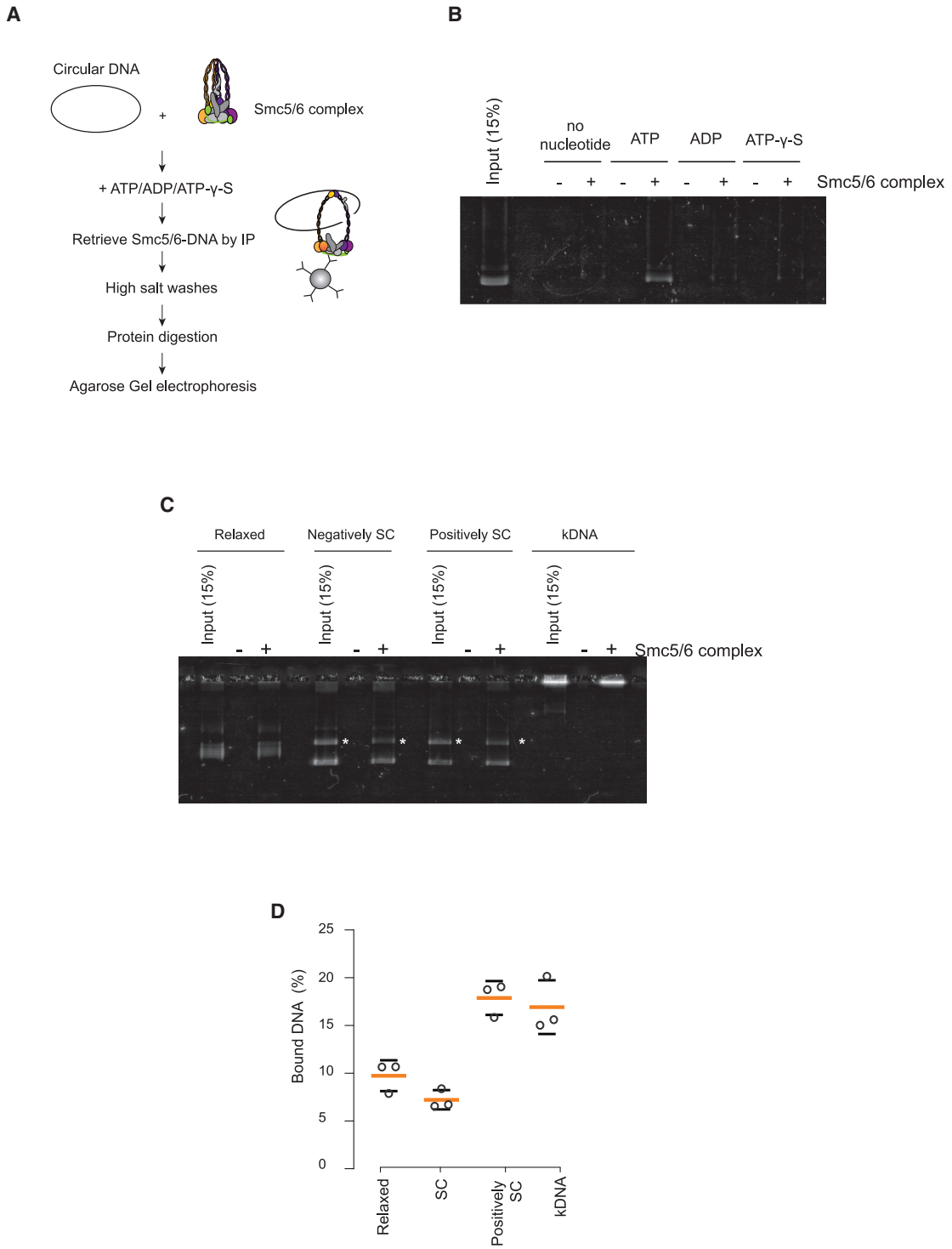

Figure 4. *In Vitro* Reconstitution of Smc5/6 Complex Topological Loading onto DNA

(A) Schematic representation of the Smc5/6 loading assay experimental design.

(B) Agarose gel electrophoresis showing recovered DNA after Smc5/6 complex loading and immunoprecipitation in the absence and presence of ATP, ADP, and ATPγS.

(legend continued on next page)

(Figure 3F) and that the Smc coiled-coils fold back at an elbow, bringing hinge regions into proximity with Smc heads. Our cross-link analysis also shows that Nse1 and Nse3 sit on top of Nse4 and interact extensively with the head domains of the Smc proteins (Figure 3F). In addition, Nse2 was found close to the elbow fold on the structure, interacting with the two coiled-coils regions on either side of the hinges (Figure 3F). Furthermore, the cross-link data of the Nse5/6 subcomplex shows that it sits between Nse2 and the Nse1/3 subunits, making substantial interactions with the base of the two Smcs (Figures 3E and 3F). The organization of Nse subunits in the structure is different from other SMC complexes, where these HEAT (Huntingtin, elongation factor 3, A subunit of protein phosphatase 2A [PP2A], signaling kinase TOR1)-repeat proteins sit below the kleisin subunit (Figures 3E and 3F).

Topological Binding of Smc5/6 Is Stimulated in Supercoiled and Catenated DNA

Smc5 and Smc6 can bind single-stranded DNA (ssDNA) and double-stranded DNA (dsDNA) as monomers (Roy and D'Amours, 2011; Roy et al., 2011) or dimers (Roy et al., 2015). Thus, we sought to investigate the DNA binding properties of purified Smc5/6 holocomplexes. We used electrophoretic mobility shift assays (EMSAs) to measure the ability of Smc5/6 complexes to bind to linear ssDNA and dsDNA templates. We incubated the substrates with increasing amounts of Smc5/6 in the presence or absence of ATP. The Smc5/6 holocomplexes were able to bind ssDNA and dsDNA in the absence of ATP, similar to the properties reported for Smc5/6 heterodimers (Roy et al., 2015). The presence of ATP clearly stimulated Smc5/6 binding to dsDNA but had a modest effect on its ability to interact with ssDNA.

Previous studies have shown that SMC complexes, including Smc5/6, can bind circular DNA in a high-salt-resistant manner (Cuylen et al., 2013; Haering et al., 2008; Kanno et al., 2015; Murayama and Uhlmann, 2014). This type of association with DNA is usually referred to as topological binding. We investigated whether our purified material was capable of topological binding. We incubated the Smc5/6 complex with relaxed circular DNA in the presence of ATP. Smc5/6 was immunoprecipitated, and after several high-salt washes (Figure 4A), we eluted and analyzed, by gel electrophoresis, the circular DNA that remained bound (Figure 4B). We observed that DNA was bound only in the presence of ATP (Figure 4B). When we digested the circular DNA, only residual binding of circular DNA was observed, demonstrating that linearization caused the majority of plasmids to escape Smc5/6. Moreover, no DNA was retained in the presence of ADP or ATPγS (adenosine 5'-gamma-thiotriphosphate) or in the absence of nucleotides (Figure 4B), indicating that topological entrapment by Smc5/6 had not taken place. Therefore, Smc5/6 DNA entrapment in this assay is strictly dependent on ATP hydrolysis. Analysis of Smc5/6 binding to yeast chromosomes shows that the localization of the complex correlates with regions containing DNA intertwines at cohesin sites (Jeppsson et al., 2014a; Sen et al., 2016). Next we sought to investigate whether DNA containing tertiary structure features, such as supercoiled and catenated DNA, were substrates for topological binding by Smc5/6. Negatively supercoiled plasmids did not stimulate topological binding compared with relaxed DNA (Figures 4C and 4D). However, catenated and positively supercoiled templates increased the amount of DNA bound topologically by Smc5/6 (Figures 4C and 4D). Collectively, these results show that topological binding by Smc5/6 has a preference for dsDNA, particularly when tertiary structures are present, such as juxtaposed DNA in the plectonemes of supercoiled plasmids and the braids of catenated dimers. It is important to note that, collectively, our EMSAs and topological binding assays demonstrate that Smc5/6 interacts with DNA by direct electrostatic interactions as well as topological entrapment.

Smc5/6 Compacts DNA Molecules against Low Physical Forces in an ATP-Dependent Manner

To investigate the real-time activity of Smc5/6 holocomplexes, we tested our purified complexes in a magnetic tweezers setup. Here linear DNA molecules are tethered between a glass surface and magnetic beads. The beads are manipulated using a pair of magnets that allows application of force and torque on the captured DNA molecules (Figure 5A). Three types of DNA substrates were captured and assayed: nicked single DNA molecules, topologically constrained single DNA molecules, and double tethered DNA molecules. These can be differentiated by the changes observed in the extension of tethered beads induced by magnet turns.

Following pre-measurements to determine the type of DNA substrate in each tether, we stretched the molecules against a constant force of 0.5 pN before injecting Smc5/6 holocomplex (10 nM) and ATP (2 mM) into the flow cell. After a lag time, we observed a progressive decrease of extension in all tether types (Figure 5B). We noticed that compaction in double tethered beads occurred significantly faster than in beads tethered with single DNA molecules (Figure 5B). Incubation with higher amounts of Smc5/6 holocomplex (52 nM) caused speed compaction to increase and a reduction of lag time. We tested whether Smc5/6 could compact DNAs against higher forces, and although we found that Smc5/6 complexes were able to compact DNAs against forces of 1 pN, the speed of compaction was significantly slower than that observed at lower forces. These results show that Smc5/6 complexes are able to condense DNA tethers, but only when the forces applied do not exceed 1 pN.

Next we tested whether Smc5/6 compaction could be reversed by applying a high force after compaction had been achieved. We applied a force of 4 pN after DNA had been initially compacted by Smc5/6 against 0.5 pN (Figure 5B). Upon force

(C) Gel image comparing the ability of the Smc5/6 complex to topologically load onto relaxed, negatively supercoiled (SC), positively SC plasmids and kinetoplast DNA (kDNA).

(D) Quantification of recovered DNA from three independent loading experiments. Mean (orange lines) and standard deviation (black lines) values are shown. Circles represent the individual measurements for each of the experiments.

See Figure S2 for further characterization of Smc5/6 DNA binding activities.

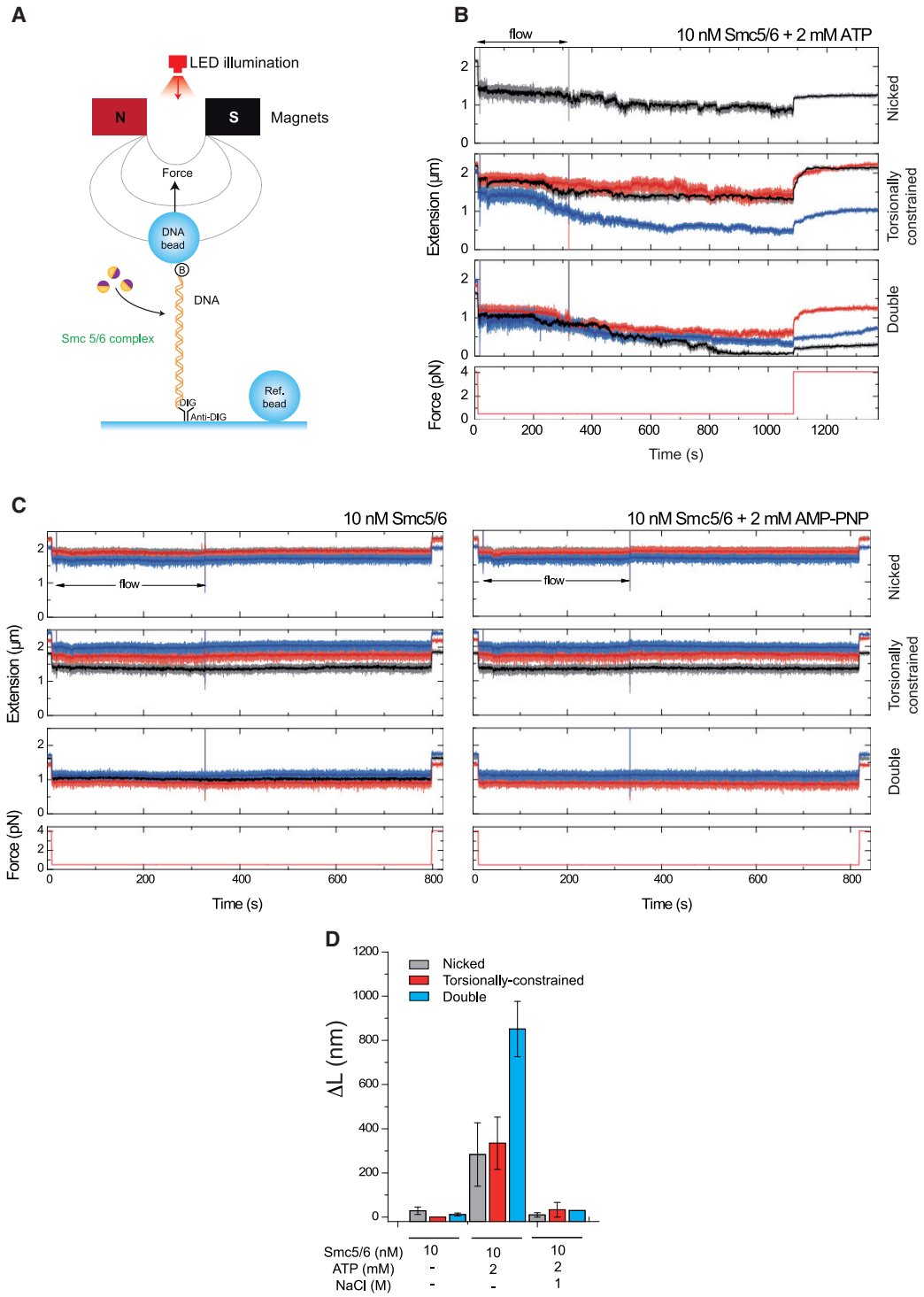

Figure 5. Single-Molecule Analysis of Smc5/6 on DNA Using MT (Magnetic Tweezers)

(A) Experimental configuration. DNA molecules are attached between a glass surface and superparamagnetic beads in a fluidics cell. Force or torque is applied by translating or rotating a pair of magnets above the chamber.

(B) Example of compaction experiments where samples containing 10 nM Smc5/6 with 2 mM ATP are introduced at 0.5 pN while monitoring the extension of different DNA tethers. Stepwise compaction (total or partial) of the tethers is observed. At the end, the force increases to 4 pN, and the initial DNA extension is only partially recovered. Traces for individual molecules are shown (red, blue, and black).

(legend continued on next page)

increase (to 4 pN), the DNA molecules largely re-extended. However, the full original extension was not recovered (Figure 5B), demonstrating that Smc5/6 complexes are able to stabilize some residual compaction even at this force. To test whether ATP binding and hydrolysis were necessary for Smc5/6 to compact DNA tethers, we investigated the activity of the complex in the absence of ATP or the presence of the non-hydrolysable ATP analog AMP-PNP. Condensation was not observed in the presence of AMP-PNP or when ATP was omitted (Figure 5C). Therefore, we conclude that Smc5/6 compaction is fully dependent on ATP. To quantify the observed compaction effect, we considered the difference between the initial and final length of DNA ($\Delta L = L_0 - L_f$) at 4 pN and after a condensation cycle (number of molecules = 39; Figure 5D). The amount of residual condensation (ΔL) was significantly larger for double tethers, confirming the preferred activity of Smc5/6 on this substrate (Figure 5D).

Next we sought to investigate whether DNA compaction by Smc5/6 occurs by electrostatic interactions or through topological binding of DNA. Electrostatic interactions should be sensitive to high salt concentrations, whereas topological association should resist high salt concentrations. Compaction induced by Smc5/6 (Figure 6A) was completely reversed in the presence of 1 M NaCl (Figures 5D and 6B). When full recovery was obtained, lowering the salt concentrations to physiological levels in the presence of ATP did not cause recompaction of the DNA tethers (Figure 6C). However, when we flowed in new Smc5/6, DNA compaction was again observed in the same molecules (Figure 6D). Therefore, this result demonstrates that DNA compaction observed in magnetic tweezers experiments does not involve topological binding of Smc5/6 to DNA.

Our gel-based results demonstrate that Smc5/6 topological binding has affinity for supercoiled and catenated substrates (Figure 4C). To study the influence of supercoiling and braiding in the compaction activity of Smc5/6, we carried out experiments introducing supercoils and braids through rotation of the magnets before adding the Smc5/6 complex (Figure 6E). We quantified DNA compaction at low force after 90 s and observed that Smc5/6 compaction was favored on supercoiled and braided substrates compared with nicked molecules. Although the supercoiling sign did not affect the compaction level, Smc5/6 compaction was increased in braided molecules. Next we investigated whether Smc5/6 could bind plectonemes present on supercoiled DNAs. We applied +30 or −30 turns to torsionally constrained DNA molecules in the presence of only ATP (Figure 6F) or ATP and Smc5/6 (Figures 6G and 6H). We then rotated the magnet back to the starting position (0 turns) and observed that the end-to-end length did not fully recover when Smc5/6 and ATP were present (Figures 6G and 6H). These results show that Smc5/6 has the ability to stabilize and lock DNA plectonemes, preventing removal through inverted rotation. Identical results were obtained regardless of the initial rotation direction, indicating that Smc5/6 can stabilize positive and negative supercoils, an ability demonstrated previously for condensin (Eeftens et al., 2017).

Given the weak DNA compaction patterns exhibited by the Smc5/6 complex, we decided to contrast Smc5/6 compaction with that of condensin under the same experimental conditions. Previous studies using magnetic tweezers have demonstrated that condensin can compact DNA (Eeftens et al., 2017; Keenholtz et al., 2017; Strick et al., 2004). We purified yeast condensin holocomplex using a protocol described previously (St-Pierre et al., 2009; Terakawa et al., 2017). First we tested whether condensin could condense DNA stretched against a constant force of 0.5 pN. We observed fast compaction of single (nicked and torsionally constrained) and double DNAs. The lag time before compaction was brief for condensin, and unlike that observed for Smc5/6, no differences between single and double DNA compaction were detected for condensin. Moreover, unlike Smc5/6, condensin compaction was not delayed significantly when we increased the stretching force to 1 pN. Our results show that condensin and Smc5/6 generate compaction through distinct mechanisms and exhibit different substrate preferences; condensin shows robust and rapid compaction of DNA against higher forces (1 pN) and, unlike Smc5/6, shows no preference for torsionally constrained or double tethers. These results suggest that Smc5/6-mediated compaction likely involves progressive stabilization of DNA tertiary structures, involving DNA crosses, which eventually causes the slow compaction of the molecules we observed.

DISCUSSION

The function of the Smc5/6 complex has traditionally been associated with DNA repair and maintenance of genomic stability. The large body of studies seeking to explore the roles of the complex has been directed toward analysis of cellular phenotypes caused by Smc5/6 deficiency. Despite these efforts, the function of Smc5/6 *in vivo* is poorly understood. Structural and biochemical characterization of the SMC complexes cohesin and condensin has provided important insights into their function and their molecular mechanism of action (Hassler et al., 2018). The number of biochemical studies of Smc5/6 is still limited. Here we purified yeast Smc5/6 holocomplexes and demonstrate that they adopt a typical double-cherry SMC-like structure, including predicted features such as folding of the coiled-coils to generate a bent stalk where the Smc hinge regions are

(C) Sequential MT experiment in which the effect of 10 nM Smc5/6 on individual traces of nicked, torsionally constrained, and double tethers is analyzed, first in the absence of ATP (left panel) and then with 2 mM AMP-PNP (a non-hydrolysable ATP analog, right panel). The samples are introduced at a low flow rate (20 μl/min) while monitoring the DNA extension. The force is maintained constant (0.5 pN) during the main part of the experiment, although the initial and final forces were 4 pN to compare DNA extensions. The measured extensions in the absence of ATP or in the presence of AMP-PNP (Adenylyl-imidodiphosphate) corresponded to those of bare DNA at each force. Traces for individual molecules are shown (red, blue, and black).
(D) Difference in the extension of DNA molecules at 4 pN measured before (L_0) and after (L_f) condensation at 0.5 pN in the presence of Smc5/6, ATP, and/or NaCl ($\Delta L = L_0 - L_f$). L_f is estimated 5 min after increasing the force to 4 pN. The effect of 1 M NaCl is quantified after condensation experiments in the presence of 10 nM Smc5/6 and ATP. Bars represent the mean ± standard error from at least two independent experiments.
See Figures S3–S5 for further characterization of Smc5/6 DNA compaction activity on magnetic tweezers.

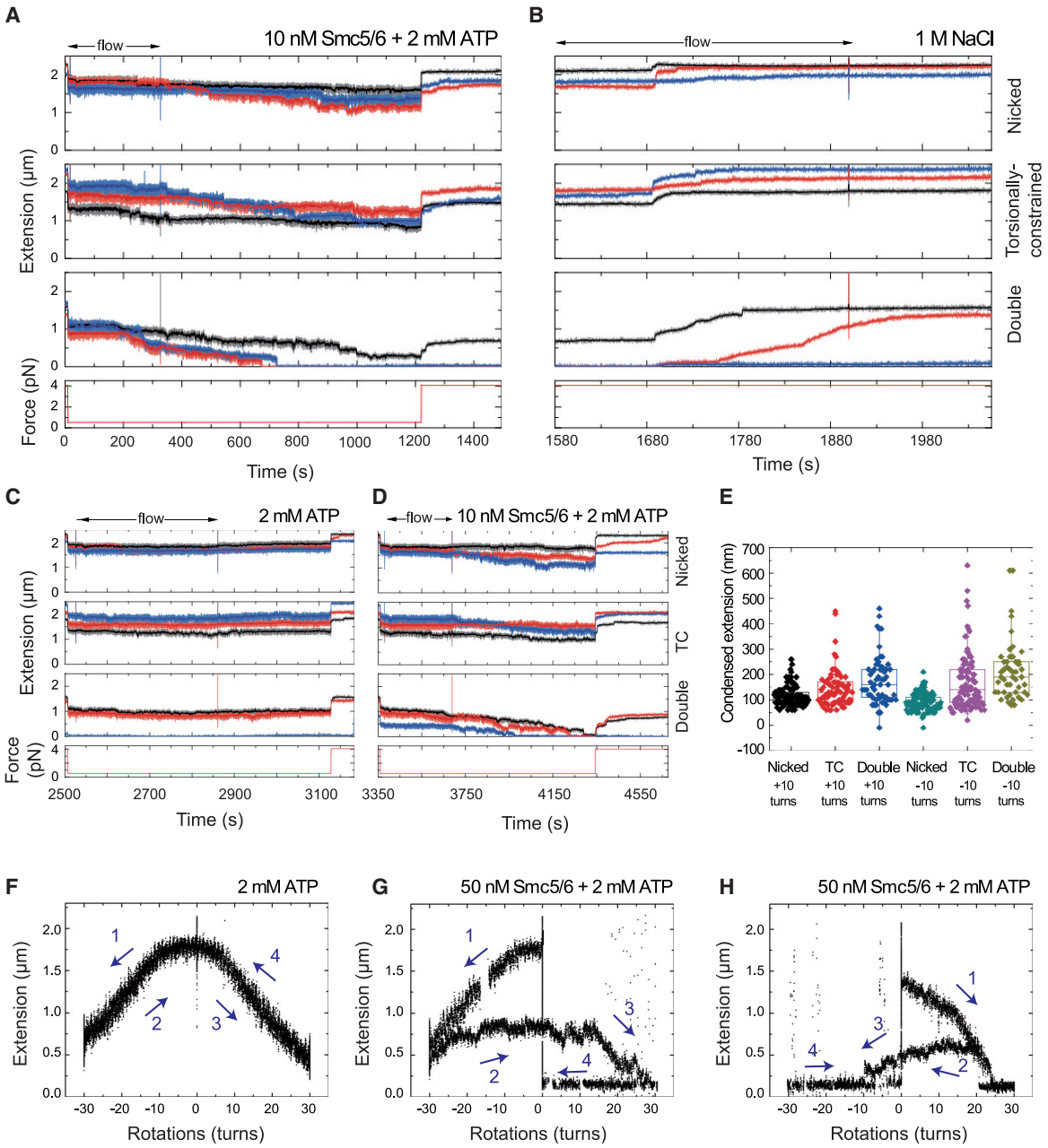

Figure 6. Smc5/6-Dependent DNA Compaction Is Sensitive to High Ionic Strength

(A) Example of a sequential experiment where a sample containing 10 nM Smc5/6 with 2 mM ATP is first introduced at 0.5 pN while monitoring the DNA extension. Stepwise compaction (total or partial) of the tethers is observed. At the end of the experiment, the force increases to 4 pN, and the initial DNA extension is only partially recovered. Traces for individual molecules are shown (red, blue, and black).

(B) The fluidics cell is then washed with a high-salt (1 M NaCl) buffer, and the DNA molecules fully recover their initial extension at 4 pN. Traces for individual molecules are shown (red, blue, and black).

(C) After washing with buffer, a solution supplemented with 2 mM ATP but no protein is added, and the force is lowered to 0.5 pN. There is no apparent compaction under these conditions. Traces for individual molecules are shown (red, blue, and black).

(D) A fresh mixture of 10 nM Smc5/6 and 2 mM ATP is added, and clear condensation is observed again. Traces for individual molecules are shown (red, blue, and black).

(E) Condensed extensions when the initial topological state of the DNA is altered by +10 or −10 turns. We allow condensation to occur for a fixed time (90 s) at low force (0.5 pN) in the presence of 10 nM Smc5/6 and 2 mM ATP.

(F) Fully reversible rotation curve of a torsionally constrained DNA molecule at 0.5 pN in the presence of 2 mM ATP. First, 30 negative rotations are applied while keeping the force constant. After 120 s at −30 turns, the magnet was turned to 30 positive rotations for another 120 s and back to 0. When turns are released (magnets at 0 rotations), the initial end-to-end distance is fully recovered.

(legend continued on next page)

proximal to the head domains. An interesting result is the position, predicted from crosslinking analysis, of the E3 SUMO ligase Nse2 within the complex. Nse2 interacts with the coiled-coil regions below the elbow (Figure 3F). Nse2-dependent SUMOylation requires ATP binding to the Smc heads (Bermúdez-López et al., 2015), indicating that global conformational changes of the Smc subunits are functionally linked to the activity of Nse2. Our results raise the possibility that the extension and bending of the coiled-coils generates distinct functional states associated with the E3 SUMO ligase activity of the complex. Cryo-EM analysis of purified yeast condensin shows different functional conformations based on the presence of ATP, where the condensin apo complex exhibits a fully folded conformation (Lee et al., 2020) while ATP binding leads to a transition of the Smc coiled-coils into a more extended architecture. Yeast cohesin has also been shown to adopt extended and folded conformations (Bürmann et al., 2019). Our EM analysis shows that the coiled-coil regions in our Smc5/6 complexes are predominantly in a folded conformation. Structural analysis of purified human Smc5/6 complexes (Serrano et al, 2020) demonstrates that coiled-coils are extended. This difference might be due to the prevalence of different conformational states in the two samples. Smc5/6 complexes are thus predicted, like condensin (Lee et al., 2020) and cohesin (Bürmann et al., 2019), to switch between extended and folded coiled-coil conformations during their nucleotide-based cycle.

Nse5 and Nse6 have been proposed to form a distinct subcomplex (Pebernard et al., 2006) that interacts with the Nse1/3/4 subunits at the base of the structure (Pebernard et al., 2006). However, another report suggested that Nse5/6 bind to the hinge regions of the Smc heterodimer (Duan et al., 2009a). Our data show that Nse5 and Nse6 have contacts with the hinge regions as well as the head regions of Smc5/6 (Figure 3E), demonstrating that these subunits are likely to bridge these two domains when the coiled-coils fold back at the elbow. Our crosslinking data indicate that kleisin Nse4 sits at the base of the structure (Figure 3E), below the Nse1 and Nse3 subunits (Figures 3E and 3F). This is in contrast to what has been observed for other SMC complexes, like condensin, where the HEAT-repeat subunits sit below the kleisin (Hassler et al., 2019).

Our crosslink MS analysis also revealed an unusually high number of crosslinks between Nse3, Nse4, and the Smc5/Smc6 head domains (Figure 3E). Moreover, mutational analysis around the N-terminal winged-helix domains in Nse3, at the center of this interaction hub, revealed direct functional relevance, with mutants exhibiting sensitivity to DNA-damaging agents (Serrano et al., 2020). Importantly, clinical relevance has been established for this region in lung disease, immunodeficiency, and chromosome breakage (LIC) syndrome (van der Crabben et al., 2016)

Previous studies have shown that Smc5/6 is able to bind circular DNA in a high-salt-resistant or topological binding manner (Kanno et al., 2015). We observed that our purified Smc5/6 holocomplex can resist high-salt washes when bound to circular plasmids (Figures 4A and 4B) and that this is dependent on the presence of ATP (Figure 4B). Previously, topological binding by Smc5/6 was assayed using nicked and negatively supercoiled plasmids, and the affinity for these substrates has been reported to be comparable (Kanno et al., 2015). We extended the analysis to plasmids that are positively supercoiled and kinetoplast DNA, which is catenated. Although Smc5/6 topological binding affinity to nicked and negatively supercoiled plasmids was similar (Figures 4C and 4D), the presence of positive supercoiling and catenation on the substrates significantly stimulated topological loading (Figures 4C and 4D). The stimulation is consistent with the idea that Smc5/6 binding sites coincide with regions where higher levels of catenation and torsional stress are present; i.e., cohesin sites in replicated chromosomes (Canela et al., 2019; Jeppsson et al., 2014a; Sen et al., 2016). In addition, we observed that Smc5/6 holocomplexes also bind ssDNA and dsDNA through direct electrostatic interactions.

Furthermore, we employed magnetic tweezers to investigate how Smc5/6 complexes associate with DNA. Our observations show that Smc5/6 is capable of compacting DNA molecules that are extended by low forces, below 1 pN (Figure 5B). Compaction requires ATP hydrolysis by the Smc5/6 pair (Figure 5C) and is sensitive to washes with high-ionic-strength buffer (Figure 6B), suggesting that compaction does not occur through topological entrapment but through electrostatic wrapping-like interactions with DNA, association between Smc5/6 complexes or is mediated by a loop extrusion mechanism (Figure 7).

We found that the rates of DNA compaction were affected by the presence of tertiary structures on the DNA substrates used (Figure 6E). Torsionally constrained DNA molecules with pre-applied turns in both directions compacted more efficiently than nicked DNA molecules (Figure 6E), and braided double DNAs also exhibited greater rates of compaction (Figure 6E). This suggests that Smc5/6 is more active when exposed to substrates that contain regions with juxtaposed DNA helices. Moreover, our results indicate that Smc5/6 is able to stabilize plectonemes on DNA substrates (Figures 6F and 6G), consistent with the idea that Smc5/6 binds preferentially to crossed DNA segments. Although Smc5/6 topological loading was favored on positively supercoiled substrates (Figures 4C and 4D), stabilization of positive and negative supercoils in our single-molecule assays was comparable (Figures 6G and 6H) consistent with the finding that compaction occurs through direct electrostatic interactions rather than topological binding. Serrano et al. (2020) report that the purified human Smc5/6 complex exhibits nearly identical behavior on single-DNA molecule magnetic tweezers as what we observed for yeast Smc5/6; namely, ATP-dependent compaction under forces not exceeding 1 pN and stabilization of supercoils of both signs. The evolutionary conservation of substrate recognition (for DNAs containing plectonemes)

(G) Example of an irreversible rotation trace obtained with the same methodology as described in (F) but in the presence of 50 nM Smc5/6 and 2 mM ATP. In this case, the original end-to-end distance is not recovered when the magnet is rotated back to 0.
(H) Similar experiment as in (G), only here positive rotations are applied first.
Numbers and arrows in (F) and (G) represent the sequence of rotations. See Figures S6 and S7 for further characterization of Smc5/6 and condensin DNA compaction activities.

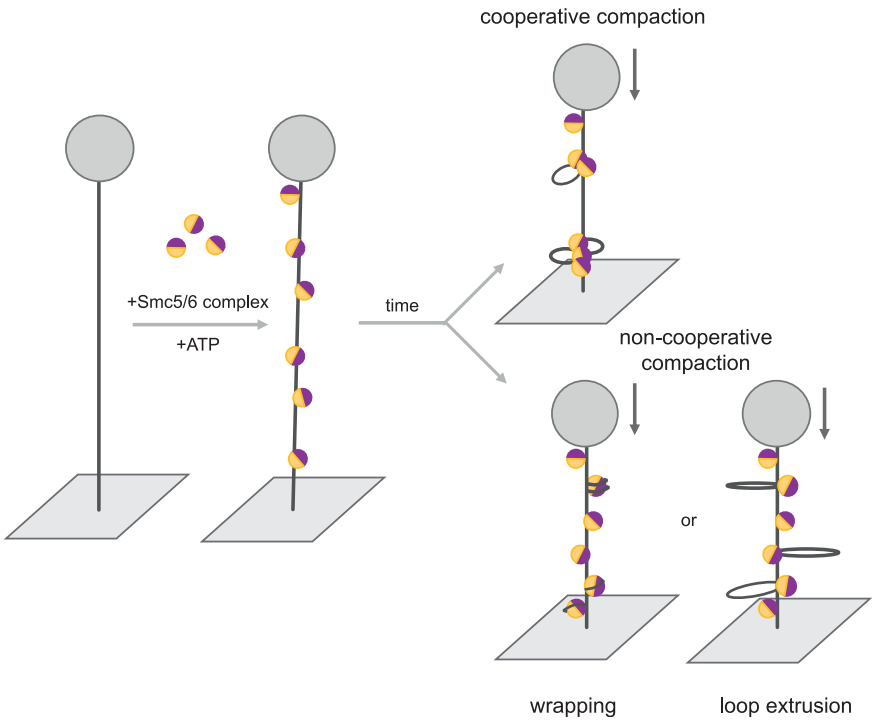

Figure 7. Models of Smc5/6 Compaction Activity

DNA compaction by the Smc5/6 complex could be achieved by cooperative or non-cooperative mechanisms. In the cooperative scenario, DNA compaction would be the result of the association between several Smc5/6 complexes. Electrostatic interactions of single complexes with the DNA (wrapping) or an extrusion-like activity of the Smc5/6 complex could explain Smc5/6 compaction activity by non-cooperative mechanisms.

suggests that this is a fundamental feature at the core of Smc5/6 function.

Presently, we do not fully understand the compaction mechanism for Smc5/6; however, we speculate that binding to juxtaposed DNAs and stabilization of DNA crosses might be an initial step. We propose that this initial step might be followed by protein-protein interactions between prebound Smc5/6 complexes or new binding of additional complexes around the sites of already prebound complexes, achieving the final compaction (Figure 7). In this scenario, greater amounts of DNA crosses in the substrate would generate an increased level of Smc5/6 bound complexes stabilizing these structures, which, in turn, would accelerate compaction as observed (Figure 6E). In addition, such a DNA compaction mechanism would be predicted to be salt sensitive because the protein-protein interactions would be disrupted in a high-ionic-strength environment. It is important to note that our results suggest that the compaction function by Smc5/6 occurs through recognition and stabilization of juxtaposed DNAs structures, present in genomic regions were DNA supercoiling or intertwines exist. It is possible that multiple Smc5/6-binding events in such genomic regions could cause local DNA compaction and facilitate processing of such structures by topoisomerases or shield the structures from nucleases and other toxic enzymatic activities.

In summary, we purified enzymatically active yeast Smc5/6 holocomplexes, characterized their structural architecture with EM, and analyzed their behavior on different DNA molecule templates using magnetic tweezers. Our data demonstrate that Smc5/6 complexes bind to substrates containing DNA tertiary structures, where crossed DNA helices are present. We propose that Smc5/6 functions as a sensor for DNA supercoiling and intertwining by recognizing and binding to crossed DNA helices. Our data also demonstrate that Smc5/6 is capable of local DNA compaction. These activities are predicted to influence or facilitate recruitment of topoisomerase activity to the DNA structures. Future analysis of the cross-talk between Smc5/6 and topoisomerase I and II should reveal whether topoisomerase recruitment/activity occurs through direct protein interactions, enzymatic activity (i.e., SUMOylation), or modulation of DNA (i.e., local compaction). Our study is a first important step towards understanding the core activity of the enigmatic Smc5/6 complex on DNA.

Limitations of Study

Finally, like every study, our work has limitations. Our structural analysis represents only one conformational state of Smc5/6, and therefore it is difficult to predict whether this structure represents a functional state on DNA. SMC complexes are dynamic machines that undergo conformational changes to perform their functions; thus, an understanding of Smc5/6 mechanisms and how these translate into specific DNA manipulations will require knowledge of all dynamic states and the binding to DNA of these.

STAR★METHODS

Detailed methods are provided in the online version of this paper and include the following:

- KEY RESOURCES TABLE
- RESOURCE AVAILABILITY
  - Lead Contact
  - Materials Availability
  - Data and Code Availability
- EXPERIMENTAL MODEL AND SUBJECT DETAILS
  - Yeast Strains
  - Strains used
  - Bacteria
  - Plasmids
- METHOD DETAILS
  - Protein expression and purification
  - ATPase assays

- Expression and purification of E1, E2 and SUMO
- *In vitro* SUMOylation reactions
- Protein cross-linking and Electron Microscopy
- Crosslinking mass spectrometry
- *In vitro* Smc5/6 loading assay
- Magnetic tweezers DNA substrate
- Magnetic tweezers assays
- ctN4 *in vitro* SUMOylation reaction
- Liquid chromatography-tandem mass spectrometry (LC-MS/MS)
- Electrophoretic gel mobility shift assay

● QUANTIFICATION AND STATISTICAL ANALYSIS

- ATPase assays
- SUMOylation assays
- DNA topological binding
- Magnetic tweezers experiments

SUPPLEMENTAL INFORMATION

Supplemental Information can be found online at https://doi.org/10.1016/j.molcel.2020.11.012.

ACKNOWLEDGMENTS

We would like to thank Chloe Roustan and Alejandra F. Cid for support during development of purification protocols. We would like to thank Roberta Corti for support and discussions of magnetic tweezers experiments. We would like to thank members of the Aragon and Moreno-Herrero laboratories for discussions and critical reading of the manuscript. We thank Prof. R. Seidel for kindly providing us with the plasmid pNLrep for DNA substrate preparation. The work in the Aragon laboratory was supported by a Wellcome Trust Senior Investigator award to L.A. (100955, "Functional dissection of mitotic chromatin") and the London Institute of Medical Research (LMS), which receives its core funding from the UK Medical Research Council (MC-A652-5PY00). F.M.-H. acknowledges support from the European Research Council (ERC) under the European Union Horizon 2020 Research and Innovation Program (grant agreement 681299). Work in the Moreno-Herrero laboratory was also supported by Spanish Ministry of Economy and Competitiveness grant BFU2017-83794-P (AEI/FEDER, UE to F.M.-H.) and Comunidad de Madrid grants Tec4-Bio – S2018/NMT-4443 and NanoBioCancer – Y2018/BIO-4747 (to F.M.-H.). Work in the J.T.-R. lab was supported by grants BFU2015-71308-P and PGC2018-097796-B-I00 from the Ministerio de Ciencia, Innovación y Universidades and grant 2017-SGR-569 from AGAUR-Generalitat de Catalunya. The IRBLLEIDA Institute is part of the CERCA Programme-Generalitat de Catalunya.

AUTHOR CONTRIBUTIONS

P.G.-E. expressed and purified yeast Smc proteins (Smc5/6 and condensin). P.G.-E. performed topological binding assays. R.S.-S. and J.T.-R. performed *in vitro* SUMOylation assays. F.J.O. and J.R. performed and analyzed cross-linking mass spectrometry experiments. K.M. and R.A. performed EM analysis. A.M. and H.K. performed mass spectrometry analysis of purified complexes. S.H. performed single-molecule magnetic tweezer experiments and analysis of data. J.M.-M. performed complementary magnetic tweezer condensation experiments. C.A.-R. produced DNA substrates for single-molecule experiments. F.M.-H. designed and supervised the single-molecule magnetic tweezer experiments. L.A. wrote the first draft of the manuscript with input from F.M.-H. All authors critically reviewed the manuscript and approved the final version. L.A. supervised the project.

DECLARATION OF INTERESTS

The authors declare no competing interests.

Received: November 22, 2019
Revised: October 12, 2020
Accepted: November 4, 2020
Published: December 9, 2020

REFERENCES

Alt, A., Dang, H.Q., Wells, O.S., Polo, L.M., Smith, M.A., McGregor, G.A., Welte, T., Lehmann, A.R., Pearl, L.H., Murray, J.M., and Oliver, A.W. (2017). Specialized interfaces of Smc5/6 control hinge stability and DNA association. Nat. Commun. *8*, 14011.

Ampatzidou, E., Irmisch, A., O'Connell, M.J., and Murray, J.M. (2006). Smc5/6 is required for repair at collapsed replication forks. Mol. Cell. Biol. *26*, 9387–9401.

Andrews, E.A., Palecek, J., Sergeant, J., Taylor, E., Lehmann, A.R., and Watts, F.Z. (2005). Nse2, a component of the Smc5-6 complex, is a SUMO ligase required for the response to DNA damage. Mol. Cell. Biol. *25*, 185–196.

Aragón, L. (2018). The Smc5/6 Complex: New and Old Functions of the Enigmatic Long-Distance Relative. Annu. Rev. Genet. *52*, 89–107.

Bermúdez-López, M., Ceschia, A., de Piccoli, G., Colomina, N., Pasero, P., Aragón, L., and Torres-Rosell, J. (2010). The Smc5/6 complex is required for dissolution of DNA-mediated sister chromatid linkages. Nucleic Acids Res. *38*, 6502–6512.

Bermúdez-López, M., Pociño-Merino, I., Sánchez, H., Bueno, A., Guasch, C., Almedawar, S., Bru-Virgili, S., Garí, E., Wyman, C., Reverter, D., et al. (2015). ATPase-dependent control of the Mms21 SUMO ligase during DNA repair. PLoS Biol. *13*, e1002089.

Bermúdez-López, M., Villoria, M.T., Esteras, M., Jarmuz, A., Torres-Rosell, J., Clemente-Blanco, A., and Aragon, L. (2016). Sgs1's roles in DNA end resection, HJ dissolution, and crossover suppression require a two-step SUMO regulation dependent on Smc5/6. Genes Dev. *30*, 1339–1356.

Bonner, J.N., Choi, K., Xue, X., Torres, N.P., Szakal, B., Wei, L., Wan, B., Arter, M., Matos, J., Sung, P., et al. (2016). Smc5/6 Mediated Sumoylation of the Sgs1-Top3-Rmi1 Complex Promotes Removal of Recombination Intermediates. Cell Rep. *16*, 368–378.

Branzei, D., Sollier, J., Liberi, G., Zhao, X., Maeda, D., Seki, M., Enomoto, T., Ohta, K., and Foiani, M. (2006). Ubc9- and mms21-mediated sumoylation counteracts recombinogenic events at damaged replication forks. Cell *127*, 509–522.

Bürmann, F., Lee, B.G., Than, T., Sinn, L., O'Reilly, F.J., Yatskevich, S., Rappsilber, J., Hu, B., Nasmyth, K., and Löwe, J. (2019). A folded conformation of MukBEF and cohesin. Nat. Struct. Mol. Biol. *26*, 227–236.

Canela, A., Maman, Y., Huang, S.N., Wutz, G., Tang, W., Zagnoli-Vieira, G., Callen, E., Wong, N., Day, A., Peters, J.M., et al. (2019). Topoisomerase II-Induced Chromosome Breakage and Translocation Is Determined by Chromosome Architecture and Transcriptional Activity. Mol. Cell *75*, 252–266.e8.

Cuylen, S., Metz, J., Hruby, A., and Haering, C.H. (2013). Entrapment of chromosomes by condensin rings prevents their breakage during cytokinesis. Dev. Cell *27*, 469–478.

Daldrop, P., Brutzer, H., Huhle, A., Kauert, D.J., and Seidel, R. (2015). Extending the range for force calibration in magnetic tweezers. Biophys. J. *108*, 2550–2561.

De Piccoli, G., Cortes-Ledesma, F., Ira, G., Torres-Rosell, J., Uhle, S., Farmer, S., Hwang, J.Y., Machin, F., Ceschia, A., McAleenan, A., et al. (2006). Smc5-Smc6 mediate DNA double-strand-break repair by promoting sister-chromatid recombination. Nat. Cell Biol. *8*, 1032–1034.

Decorsière, A., Mueller, H., van Breugel, P.C., Abdul, F., Gerossier, L., Beran, R.K., Livingston, C.M., Niu, C., Fletcher, S.P., Hantz, O., and Strubin, M. (2016). Hepatitis B virus X protein identifies the Smc5/6 complex as a host restriction factor. Nature *531*, 386–389.

Deiss, K., Lockwood, N., Howell, M., Segeren, H.A., Saunders, R.E., Chakravarty, P., Soliman, T.N., Martini, S., Rocha, N., Semple, R., et al. (2019). A genome-wide RNAi screen identifies the SMC5/6 complex as a

non-redundant regulator of a Topo2a-dependent G2 arrest. Nucleic Acids Res. *47*, 2906–2921.

Duan, X., Sarangi, P., Liu, X., Rangi, G.K., Zhao, X., and Ye, H. (2009a). Structural and functional insights into the roles of the Mms21 subunit of the Smc5/6 complex. Mol. Cell *35*, 657–668.

Duan, X., Yang, Y., Chen, Y.H., Arenz, J., Rangi, G.K., Zhao, X., and Ye, H. (2009b). Architecture of the Smc5/6 Complex of Saccharomyces cerevisiae Reveals a Unique Interaction between the Nse5-6 Subcomplex and the Hinge Regions of Smc5 and Smc6. J. Biol. Chem. *284*, 8507–8515.

Eeftens, J.M., Bisht, S., Kerssemakers, J., Kschonsak, M., Haering, C.H., and Dekker, C. (2017). Real-time detection of condensin-driven DNA compaction reveals a multistep binding mechanism. EMBO J. *36*, 3448–3457.

Fili, N., Mashanov, G.I., Toseland, C.P., Batters, C., Wallace, M.I., Yeeles, J.T., Dillingham, M.S., Webb, M.R., and Molloy, J.E. (2010). Visualizing helicases unwinding DNA at the single molecule level. Nucleic Acids Res. *38*, 4448–4457.

Fischer, L., and Rappsilber, J. (2017). Quirks of Error Estimation in Cross-Linking/Mass Spectrometry. Anal. Chem. *89*, 3829–3833.

Gallego-Paez, L.M., Tanaka, H., Bando, M., Takahashi, M., Nozaki, N., Nakato, R., Shirahige, K., and Hirota, T. (2014). Smc5/6-mediated regulation of replication progression contributes to chromosome assembly during mitosis in human cells. Mol. Biol. Cell *25*, 302–317.

Haering, C.H., Farcas, A.M., Arumugam, P., Metson, J., and Nasmyth, K. (2008). The cohesin ring concatenates sister DNA molecules. Nature *454*, 297–301.

Hassler, M., Shaltiel, I.A., and Haering, C.H. (2018). Towards a Unified Model of SMC Complex Function. Curr. Biol. *28*, R1266–R1281.

Hassler, M., Shaltiel, I.A., Kschonsak, M., Simon, B., Merkel, F., Tharichen, L., Bailey, H.J., Macosek, J., Bravo, S., Metz, J., et al. (2019). Structural Basis of an Asymmetric Condensin ATPase Cycle. Mol. Cell *74*, 1175–1188.e9.

Hay, R.T. (2001). Protein modification by SUMO. Trends Biochem. Sci. *26*, 332–333.

Hirano, T. (2005). SMC proteins and chromosome mechanics: from bacteria to humans. Philos. Trans. R. Soc. Lond. B Biol. Sci. *360*, 507–514.

Irmisch, A., Ampatzidou, E., Mizuno, K., O'Connell, M.J., and Murray, J.M. (2009). Smc5/6 maintains stalled replication forks in a recombination-competent conformation. EMBO J. *28*, 144–155.

Jeppsson, K., Carlborg, K.K., Nakato, R., Berta, D.G., Lilienthal, I., Kanno, T., Lindqvist, A., Brink, M.C., Dantuma, N.P., Katou, Y., et al. (2014a). The chromosomal association of the Smc5/6 complex depends on cohesion and predicts the level of sister chromatid entanglement. PLoS Genet. *10*, e1004680.

Jeppsson, K., Kanno, T., Shirahige, K., and Sjögren, C. (2014b). The maintenance of chromosome structure: positioning and functioning of SMC complexes. Nat. Rev. Mol. Cell Biol. *15*, 601–614.

Johnson, E.S., and Gupta, A.A. (2001). An E3-like factor that promotes SUMO conjugation to the yeast septins. Cell *106*, 735–744.

Kanno, T., Berta, D.G., and Sjögren, C. (2015). The Smc5/6 Complex Is an ATP-Dependent Intermolecular DNA Linker. Cell Rep. *12*, 1471–1482.

Keenholtz, R.A., Dhanaraman, T., Palou, R., Yu, J., D'Amours, D., and Marko, J.F. (2017). Oligomerization and ATP stimulate condensin-mediated DNA compaction. Sci. Rep. *7*, 14279.

Kolbowski, L., Mendes, M.L., and Rappsilber, J. (2017). Optimizing the Parameters Governing the Fragmentation of Cross-Linked Peptides in a Tribrid Mass Spectrometer. Anal. Chem. *89*, 5311–5318.

Lee, B.G., Merkel, F., Allegretti, M., Hassler, M., Cawood, C., Lecomte, L., O'Reilly, F.J., Sinn, L.R., Gutierrez-Escribano, P., Kschonsak, M., et al. (2020). Cryo-EM structures of holo condensin reveal a subunit flip-flop mechanism. Nat. Struct. Mol. Biol. *27*, 743–751.

Lenz, S., Giese, S.H., Fischer, L., and Rappsilber, J. (2018). In-Search Assignment of Monoisotopic Peaks Improves the Identification of Cross-Linked Peptides. J. Proteome Res. *17*, 3923–3931.

Lindroos, H.B., Ström, L., Itoh, T., Katou, Y., Shirahige, K., and Sjögren, C. (2006). Chromosomal association of the Smc5/6 complex reveals that it functions in differently regulated pathways. Mol. Cell *22*, 755–767.

Losada, A., and Hirano, T. (2005). Dynamic molecular linkers of the genome: the first decade of SMC proteins. Genes Dev. *19*, 1269–1287.

McAleenan, A., Cordon-Preciado, V., Clemente-Blanco, A., Liu, I.C., Sen, N., Leonard, J., Jarmuz, A., and Aragón, L. (2012). SUMOylation of the α-kleisin subunit of cohesin is required for DNA damage-induced cohesion. Curr. Biol. *22*, 1564–1575.

Mendes, M.L., Fischer, L., Chen, Z.A., Barbon, M., O'Reilly, F.J., Giese, S.H., Bohlke-Schneider, M., Belsom, A., Dau, T., Combe, C.W., et al. (2019). An integrated workflow for crosslinking mass spectrometry. Mol. Syst. Biol. *15*, e8994.

Menolfi, D., Delamarre, A., Lengronne, A., Pasero, P., and Branzei, D. (2015). Essential Roles of the Smc5/6 Complex in Replication through Natural Pausing Sites and Endogenous DNA Damage Tolerance. Mol. Cell *60*, 835–846.

Murayama, Y., and Uhlmann, F. (2014). Biochemical reconstitution of topological DNA binding by the cohesin ring. Nature *505*, 367–371.

Murphy, C.M., Xu, Y., Li, F., Nio, K., Reszka-Blanco, N., Li, X., Wu, Y., Yu, Y., Xiong, Y., and Su, L. (2016). Hepatitis B Virus X Protein Promotes Degradation of SMC5/6 to Enhance HBV Replication. Cell Rep. *16*, 2846–2854.

Nasmyth, K., and Haering, C.H. (2005). The structure and function of SMC and kleisin complexes. Annu. Rev. Biochem. *74*, 595–648.

Palecek, J., Vidot, S., Feng, M., Doherty, A.J., and Lehmann, A.R. (2006). The Smc5-Smc6 DNA repair complex. bridging of the Smc5-Smc6 heads by the KLEISIN, Nse4, and non-Kleisin subunits. J. Biol. Chem. *281*, 36952–36959.

Pebernard, S., Wohlschlegel, J., McDonald, W.H., Yates, J.R., 3rd, and Boddy, M.N. (2006). The Nse5-Nse6 dimer mediates DNA repair roles of the Smc5-Smc6 complex. Mol. Cell. Biol. *26*, 1617–1630.

Potts, P.R., and Yu, H. (2005). Human MMS21/NSE2 is a SUMO ligase required for DNA repair. Mol. Cell. Biol. *25*, 7021–7032.

Potts, P.R., Porteus, M.H., and Yu, H. (2006). Human SMC5/6 complex promotes sister chromatid homologous recombination by recruiting the SMC1/3 cohesin complex to double-strand breaks. EMBO J. *25*, 3377–3388.

Rappsilber, J., Ishihama, Y., and Mann, M. (2003). Stop and go extraction tips for matrix-assisted laser desorption/ionization, nanoelectrospray, and LC/MS sample pretreatment in proteomics. Anal. Chem. *75*, 663–670.

Roy, M.A., and D'Amours, D. (2011). DNA-binding properties of Smc6, a core component of the Smc5-6 DNA repair complex. Biochem. Biophys. Res. Commun. *416*, 80–85.

Roy, M.A., Siddiqui, N., and D'Amours, D. (2011). Dynamic and selective DNA-binding activity of Smc5, a core component of the Smc5-Smc6 complex. Cell Cycle *10*, 690–700.

Roy, M.A., Dhanaraman, T., and D'Amours, D. (2015). The Smc5-Smc6 heterodimer associates with DNA through several independent binding domains. Sci. Rep. *5*, 9797.

Seidel, R., van Noort, J., van der Scheer, C., Bloom, J.G., Dekker, N.H., Dutta, C.F., Blundell, A., Robinson, T., Firman, K., and Dekker, C. (2004). Real-time observation of DNA translocation by the type I restriction modification enzyme EcoR124I. Nat. Struct. Mol. Biol. *11*, 838–843.

Sen, N., Leonard, J., Torres, R., Garcia-Luis, J., Palou-Marin, G., and Aragón, L. (2016). Physical Proximity of Sister Chromatids Promotes Top2-Dependent Intertwining. Mol. Cell *64*, 134–147.

Sergeant, J., Taylor, E., Palecek, J., Fousteri, M., Andrews, E.A., Sweeney, S., Shinagawa, H., Watts, F.Z., and Lehmann, A.R. (2005). Composition and architecture of the Schizosaccharomyces pombe Rad18 (Smc5-6) complex. Mol. Cell. Biol. *25*, 172–184.

Serrano, D., Cordero, G., Kawamura, R., Sverzhinsky, A., Sarker, M., Roy, S., Malo, C., Pascal, J.M., Marko, J.F., and D'Amours, D. (2020). The Smc5/6 Core Complex Is a Structure-Specific DNA Binding and Compacting Machine. Mol Cell *80*, this issue, 1025–1038.

St-Pierre, J., Douziech, M., Bazile, F., Pascariu, M., Bonneil, E., Sauvé, V., Ratsima, H., and D'Amours, D. (2009). Polo kinase regulates mitotic chromosome condensation by hyperactivation of condensin DNA supercoiling activity. Mol. Cell *34*, 416–426.

Strick, T.R., Allemand, J.F., Bensimon, D., and Croquette, V. (1998). Behavior of supercoiled DNA. Biophys. J. *74*, 2016–2028.

Strick, T.R., Kawaguchi, T., and Hirano, T. (2004). Real-time detection of single-molecule DNA compaction by condensin I. Curr. Biol. *14*, 874–880.

Terakawa, T., Bisht, S., Eeftens, J.M., Dekker, C., Haering, C.H., and Greene, E.C. (2017). The condensin complex is a mechanochemical motor that translocates along DNA. Science *358*, 672–676.

Torres-Rosell, J., Machín, F., Farmer, S., Jarmuz, A., Eydmann, T., Dalgaard, J.Z., and Aragón, L. (2005). SMC5 and SMC6 genes are required for the segregation of repetitive chromosome regions. Nat. Cell Biol. *7*, 412–419.

Torres-Rosell, J., De Piccoli, G., Cordon-Preciado, V., Farmer, S., Jarmuz, A., Machin, F., Pasero, P., Lisby, M., Haber, J.E., and Aragón, L. (2007). Anaphase onset before complete DNA replication with intact checkpoint responses. Science *315*, 1411–1415.

van der Crabben, S.N., Hennus, M.P., McGregor, G.A., Ritter, D.I., Nagamani, S.C., Wells, O.S., Harakalova, M., Chinn, I.K., Alt, A., Vondrova, L., et al. (2016). Destabilized SMC5/6 complex leads to chromosome breakage syndrome with severe lung disease. J. Clin. Invest. *126*, 2881–2892.

Varejão, N., Ibars, E., Lascorz, J., Colomina, N., Torres-Rosell, J., and Reverter, D. (2018). DNA activates the Nse2/Mms21 SUMO E3 ligase in the Smc5/6 complex. EMBO J. *37*, e98306.

Wu, N., Kong, X., Ji, Z., Zeng, W., Potts, P.R., Yokomori, K., and Yu, H. (2012). Scc1 sumoylation by Mms21 promotes sister chromatid recombination through counteracting Wapl. Genes Dev. *26*, 1473–1485.

Xu, W., Ma, C., Zhang, Q., Zhao, R., Hu, D., Zhang, X., Chen, J., Liu, F., Wu, K., Liu, Y., and Wu, J. (2018). PJA1 Coordinates with the SMC5/6 Complex To Restrict DNA Viruses and Episomal Genes in an Interferon-Independent Manner. J. Virol. *92*, e00825-18.

Zhao, X., and Blobel, G. (2005). A SUMO ligase is part of a nuclear multiprotein complex that affects DNA repair and chromosomal organization. Proc. Natl. Acad. Sci. USA *102*, 4777–4782.

STAR★METHODS

KEY RESOURCES TABLE

REAGENT or RESOURCE	SOURCE	IDENTIFIER
Antibodies		
Mouse monoclonal anti-HA (12CA5)	Sigma-Aldrich	Sigma-Aldrich Cat# 11583816001, RRID:AB_514505
Anti-Smt3	Abcam	Abcam Cat# ab14405, RRID:AB_301186
Anti-rabbit IgG (HRP-conjugated)	Thermo Fisher Scientific	Thermo Fisher Scientific Cat# 10710965, RRID:AB_772191
Anti-mouse IgG (HRP-conjugated)	GE Healthcare	GE Healthcare Cat# NA931, RRID:AB_772210
Bacterial and Virus Strains		
Stbl2 *E.coli*	Invitrogen	Cat#10268019
Rosetta 2 (DE3) pLysS *E.coli*	Sigma-Aldrich	Cat#CMC0014
Chemicals, Peptides, and Recombinant Proteins		
DTT	Sigma-Aldrich	Cat#43815-5G
ATP	Sigma-Aldrich	Cat#A2383
biotin	Sigma-Aldrich	Cat#B4501-1G
cOmplete EDTA-Free protease inhibitor cocktail	Sigma-Aldrich	Cat#11873580001
BSA	Thermo Fisher	Cat#AM2616
Benzonase	Sigma-Aldrich	Cat#1000.01695.0001
Desthiobiotin	Sigma-Aldrich	Cat#D1411-1G
InstantBlue	Sigma-Aldrich	Cat#IBSL-1L
NuPAGE 4-12% Protein gels	Thermo-Fisher	Cat#NP0321PK2
Amicon Ultra	Sigma-Aldrich	Cat#UFC5003
Phospho(enol)pyruvic acid	Sigma-Aldrich	Cat#P7127
Pyruvate kinase	Sigma-Aldrich	Cat#P9136
Lactate dehydrogenase	Sigma-Aldrich	Cat#SAE0049
NADH	Sigma-Aldrich	Cat#10107735001
β-mercaptoethanol	Sigma-Aldrich	Cat#M6250
Imidazole	Sigma-Aldrich	Cat#I2399
Oriole Gel stain	BioRad	Cat#161-0495
SYBR Safe gel stain	Thermofisher	Cat#S33102
Critical Commercial Assays		
StrepTrap HP	Cytivia	Cat#28907548
HiTrap Heparin HP 5ml	Cytivia	Cat#GE17-0407-01
Superose 6 10/300 GL	GE Healthcare	Cat#17517201
Ni-NTA Superflow	QIAGEN	Cat#30410
Dynabeads MyOne Streptavidin	ThermoFisher	Cat#65601
Deposited Data		
Protein-protein crosslink mass spectrometry (CLMS) data	PRIDE	PXD016196
Experimental Models: Organisms/Strains		
Yeast strain: *Mata Lys2::pGAL1-GAL4::LYS2 pep4::HIS3 bar1::hisG ade2-1 trp1D2 can1-100 leu 2-3,112*	Aragon lab	n/a
Yeast strain: *CCG14584 -Mata Lys2::pGAL1-GAL4::LYS2 pep4::HIS3 bar1::hisG ade2-1 trp1D2 can1-100 leu 2-3,112 [pRS424-GAL-SMC6-3xStrepII-SMC5-NSE4-His-3HA] [pRS426-GAL-NSE1-NSE3-NSE6-NSE2-NSE5]*	Aragon lab	n/a

(*Continued on next page*)

Continued

REAGENT or RESOURCE	SOURCE	IDENTIFIER
Yeast strain: *CCG14619 -Mata Lys2::pGAL1-GAL4::LYS2 pep4::HIS3 bar1::hisG ade2-1 trp1D2 can1-100 leu 2-3,112 [pRS424-GAL-SMC6-3xStrepII-SMC5-NSE4-His-3HA] [pRS426-GAL-NSE1-NSE3-NSE6-NSE2-NSE5].*	Aragon lab	n/a
Oligonucleotides		
Magnetic tweezers oligo 1 5′GCGTAAGTGGTACCTT ATAAAGTACTCGACTCAC TATAGGGAGACCGGC-3′	Sigma-Aldrich	n/a
Magnetic tweezers oligo 2 5′-AGTAAGCGCCGTCAGACCAG-3′	Sigma-Aldrich	n/a
Recombinant DNA		
Plasmid- CCG1198 [pRS424-GAL1-SMC6-3xStrepII-SMC5-NSE4-His-3HA TRP1]	Aragon lab	n/a
Plasmid- CCG1204 [pRS426-GAL1-NSE1-NSE3-NSE6-NSE2-NSE5 URA3]	Aragon lab	n/a
Plasmid- CCG1267 [pRS426-GAL-SMC4StrepII-SMC2-BRN1-His6-3HA URA3]	Haering lab	Terakawa et al. 2017
Plasmid- CCG1268 [pRS424-GAL-YCS4-YCG1 TRP1]	Haering lab	Terakawa et al. 2017
Software and Algorithms		
xiVIEV	Rappsilber lab	N/A
MaxQuant	Max Planck, Martinsried, Germany	https://maxquant.org
OriginPro 8	Originlab Corporation	https://www.originlab.com/
LabVIEW software	Moreno-Herrero lab	N/A
RELION	Scheres lab	https://www2.mrc-lmb.cam.ac.uk/groups/scheres/impact.html
Image Lab	BioRad	Cat#17006130
Fiji ImageJ	Open source	https://imageJ.net/Fiji
Other		
Negatively supercoiled pBR322	Inspiralis	Cat#S5001
Positively supercoiled pBR322	Inspiralis	Cat#POS5001
Catenated DNA (kDNA)	Inspiralis	Cat#K2001

RESOURCE AVAILABILITY

Lead Contact

Further information for resources and requests should be directed to and will be fulfilled by the Lead Contact, Luis Aragon (luis.aragon@lms.mrc.ac.uk)

Materials Availability

All reagents generated in this study are available from the Lead Contact without restriction.

Data and Code Availability

The CLMS data have been deposited to the ProteomeXchange Consortium. PRIDE:PXD016196.

EXPERIMENTAL MODEL AND SUBJECT DETAILS

Yeast Strains

The Smc5/6 holocomplex and condensin pentamer complexes were expressed in W303 background *Saccharomyces cerevisiae* strain.

Strains used

CCG14584 -Mata Lys2::pGAL1-GAL4::LYS2 pep4::HIS3 bar1::hisG ade2-1 trp1D2 can1-100 leu 2-3,112 [pRS424-GAL-SMC6-3xStrepII-SMC5-NSE4-His-3HA] [pRS426-GAL-NSE1-NSE3-NSE6-NSE2-NSE5]

CCG14619 -Mata Lys2::pGAL1-GAL4::LYS2 pep4::HIS3 bar1::hisG ade2-1 trp1D2 can1-100 leu 2-3,112 [pRS424-GAL-SMC6-3xStrepII-SMC5-NSE4-His-3HA] [pRS426-GAL-NSE1-NSE3-NSE6-NSE2-NSE5].

Bacteria

Plasmids for expression of SMC complexes were amplified in JM109 *E.coli* strains Stbl2 (F^- *mcr*A Δ(*mcr*BC-hsdRMS-*mrr*) *rec*A1 *end*A1*lon gyr*A96 *thi sup*E44 *rel*A1 λ^- Δ(*lac-pro*AB) (invitrogen).

Plasmids

Plasmids for expression of SMC complexes:

CCG1198 [pRS424-GAL1-SMC6-3xStrepII-SMC5-NSE4-His-3HA TRP1] CCG1204 [pRS426-GAL1-NSE1-NSE3-NSE6-NSE2-NSE5 URA3] CCG1267 [pRS426-GAL-SMC4StrepII-SMC2-BRN1-His6-3HA URA3] CCG1268 [pRS424-GAL-YCS4-YCG1 TRP1]

METHOD DETAILS

Protein expression and purification

The different subunits of the *S. cerevisiae* Smc5/6 were synthesized under the control of galactose inducible promoters and cloned into multicopy episomal vectors (*URA3-GAL-NSE1-NSE2-NSE3-NSE5-NSE6 and TRP1-GAL-SMC6-3xStrepII-SMC5-NSE4-8xHis-3xHA).* Budding yeast W303-1a strains carrying both constructs (CCG14854) were grown at 30°C in selective dropout media containing 2% raffinose and 0.1% Glucose to OD_{600} of 1. Protein expression was induced by addition of 2% galactose and cells were grown for further 16 hours at 20°C. Cells were then harvested by centrifugation at 4°C, resuspended in 2/3 volumes of buffer A (25 mM HEPES pH 7.5, 200 mM NaCl, 5% glycerol, 5 mM β-mercaptoethanol) containing 1 × cOmplete™ EDTA-free protease-inhibitor mix (Sigma-Aldrich), frozen in liquid nitrogen and lysed in a FreezerMill (SPEX Certiprep 6870). Cell powder was thawed at 4°C for 2 hours before mixing it with 1/3 volume of buffer A containing benzonase (Millipore) and incubated at 4°C for an extra hour. Cell lysates were clarified by centrifugation at 45 000 g for 1 hour followed by filtration using 0.22 μm syringe filters. Clarified lysates were loaded onto 5ml StrepTrap-HP columns (Cytivia) pre-equilibrated with buffer A. The resin was washed with 5 column volumes of buffer A and eluted with buffer B (buffer A containing 5mM desthiobiotin). The peak fractions containing the overexpressed proteins were pooled together and salt concentration was adjusted to 150 mM NaCl using 100 mM NaCl-buffer A. Samples were then filtered as described above to remove residual aggregates and loaded onto 5ml HiTrap Heparin HP (GE Healthcare) columns pre-equilibrated with 150mM NaCl-buffer A. Elution was carried out using a linear gradient from 150 mM to 1 M NaCl in buffer A. Peak fractions were pooled and concentrated by centrifugal ultrafiltration (100 kDa Amicon Ultra, Millipore). Salt concentration was adjusted to 300 mM NaCl during the concentration step. Gel Filtration was carried out using a Superose 6 Increase 100/300 GL column (GE Healthcare) in 300 mM NaCl buffer A. Fractions corresponding to monomeric complexes were pooled and concentrated as described above. Purified proteins were analyzed by SDS-PAGE (NuPAGE 4%–12% Bis-Tris protein gels, ThermoFisher Scientific) and Coomassie staining (InstantBlue, Expedeon). Protein identification was carried out by mass spectrometry analysis. *S. cerevisiae* condensin complex was expressed and purified as previously described (St-Pierre et al., 2009; Terakawa et al., 2017). See Table S1 for further characterization of Smc5/6 purifications.

ATPase assays

ATPase activity of the purified Smc5/6 complex was measured using an ATP/NADH coupled assay in a spectrophotometer (LAMBDA 365 UV/Vis, PerkinElmer). The buffer for the experiments contained 50 mM NaCl, 40 mM Tris-HCl pH 7.5, 7 mM $MgCl_2$, 3 mM DTT, as well as 0.5 mM phospho(enol)pyruvic acid, 200 U/ml pyruvate kinase, 200 U/ml lactate dehydrogenase, 80 μg/ml NADH and 2 mM ATP. We tested Smc5/6 alone (without DNA) and in the presence of a circular plasmid with a 63-nt-gap (pNLrep, 6895 bp). The protein:DNA ratio was 4.87:1 in the final volume. The initial ATP concentration was 2 mM.

Expression and purification of E1, E2 and SUMO

Ubc9 and Smt3 expression were induced in Rosetta 2 (DE3) pLysS cells (Novagen) at an OD600 of 0,6 by addition of IPTG 1 mM for 4 hours at 37°C. For Ubc9 purification, cells were recovered by centrifugation at 5000 g, resuspended in lysis buffer (50 mM NaCl, 50 mM KPO_4, pH 6.5) and frozen at −80°C. Pellets were thawed in the presence of protease inhibitors and 5 mM β-mercaptoethanol and spun at 100.000 g for 1 hour at 4°C. After centrifugation, the supernatant was passed through a 0.2 μm filter. Next, imidazole was added to 20 mM and incubated with 500 μL NiNTA beads prewashed in washing buffer (50 mM NaCl, 50 mM sodium phosphate, pH 6.5, 20 mM imidazole, 5mM β-mercaptoethanol). After binding, beads were washed 3 times with washing buffer and Ubc9 was eluted in washing buffer containing 300 mM NaCl and 250 mM imidazole. Finally, the sample was dialyzed against 10% glycerol, 50 mM HEPES pH 7, 100 mM NaCl, 10 mM $MgCl_2$, 20 mM imidazole, 0,5 μM $ZnCl_2$. For Smt3 purification, cells were recovered by centrifugation at 5.000 g and frozen at −80°C. Next, pellets were cryogenically disrupted in a ball mill and the pulverized material was resuspended in extraction buffer (300 mM NaCl, 50 mM Tris-HCl pH 8, 50 mM KPO_4 pH 8, 0.5% NP-40, 5 mM β-mercaptoethanol and protease inhibitors). The sample was sonicated and spun at 75.000 g for one hour at 4°C. The supernatant was passed through a 0,2 μm filter, and imidazole was added to 20 mM. Next, the extract was incubated with 500 μL of NiNTA beads prewashed with

washing buffer (50 mM Tris-HCl pH 8, 50 mM KPO_4 pH 8, 5% glycerol, 5 mM β-mercaptoethanol, 300 mM NaCl, 20 mM imidazole and protease inhibitors). After binding, beads were washed 2 times with washing buffer, and eluted in washing buffer containing 250 mM imidazole. The sample was finally dialyzed against the same buffer used for Ubc9. E1 was expressed and purified as described in Johnson and Gupta (2001).

In vitro SUMOylation reactions

For Smc5/6 SUMOylation reactions, 165 nM Smc5/6 was mixed with 150 nM E1, 100 nM E2 and 16 μM Smt3 in reaction buffer containing 40 mM HEPES pH 7.5, 10 mM $MgCl_2$, 50 mM NaCl and 0.2% Tween-20. Supercoiled DNA was added to a final concentration of 10 mM in the reactions stimulated with DNA. Reactions were started by addition of 2 mM ATP, incubated at 30°C for 15 minutes and stopped with SDS-PAGE loading buffer (4% SDS, 10% sucrose, 0.025% bromophenol blue and 1% 2-mercaptoethanol in 0.25 M Tris-HCl pH 6.8). The products were analyzed by SDS-PAGE followed by Oriole staining (BioRad) or Western Blot with anti-Smt3 (Abcam). Conjugated and free SUMO were quantified using Image Lab (Bio-Rad).

Protein cross-linking and Electron Microscopy

For cross-linking of Smc5/6 complex, samples at a concentration of 0.08 mg/mL were cross-linked in 25 mM HEPES pH8, 125 mM NaCl, 5% glycerol, 1 mM DTT at a ratio of 1:600 using BS3 for 2 hours at 4°C. The cross-linking reaction was quenched using 100 mM Tris-HCl pH 8. The cross-linked complex was applied to glow discharged continuous carbon EM grids at 0.02 mg/mL and adsorbed for 1 minute. Sample was blotted and the grid negatively stained two times using 2% w/v Uranyl Acetate for 1 minute. The negatively stained complex was visualized using a Philips CM200 operated at 160 kV and TVIPS TemCam F216. Particles were picked using gautomatch and 2D averaging performed in Relion-3.0.

Grids for cryo-electron microscopy were prepared by depositing 3.5 μl of the diluted sample (dilution half, with a final concentration of 0.44 mg/ml at 4°C) onto Quantifoil R2/2 copper grids. Samples were blotted before being frozen in liquid ethane at liquid nitrogen temperature with a FEI Vitrobot Mark IV. Micrographs were collected on a Tecnai F20 FEG microscope operated at 200 kV. Images were recorded on a Falcon II direct electron detector at a nominal magnification of 62,000 (final pixel size of 1.65 Å/pixel). The total dose was 40 $e^{-}/Å^2$. A total of 1,400 particles was extracted and binned into boxes of 180x180 pixels with pixel size 3.30 Å. CTF parameters were estimated with gCTF software. Particles were picked using gautomatch and 2D averaging performed in Relion-3.0.

Crosslinking mass spectrometry

For crosslinking mass spectrometry analysis, 130 μg of Smc5/6 complex was crosslinked using a 1:600 molar ratio of protein to BS3 as described above. Quenching was achieved by addition of 50mM Ammonium Bicarbonate and incubation for 30 min at temperature. Reaction products were separated by SDS-PAGE as described above. The gel band corresponding to the cross-linked species was excised and digested with trypsin (Pierce, Germany). The resulting tryptic peptides were extracted and desalted using C18 StageTips (Rappsilber et al., 2003). Eluted peptides were fractionated on an ÄKTA Pure system (GE Healthcare) using a Superdex Peptide 3.2/300 (GE Healthcare) at a flow rate of 10 μL/min using 30% (v/v) acetonitrile and 0.1% (v/v) trifluoroacetic acid as mobile phase. Five 50 μl fractions were collected and dried.

Samples for analysis were resuspended in 0.1% (v/v) formic acid 1.6% (v/v) acetonitrile. LC-MS/MS analysis was conducted in duplicate for SEC fractions and triplicate for SCX fractions, performed on an Orbitrap Fusion Lumos Tribrid mass spectrometer (Thermo Fisher Scientific, Germany) coupled on-line with an Ultimate 3000 RSLCnano system (Dionex, Thermo Fisher Scientific, Germany). The sample was separated and ionized by a 50 cm EASY-Spray column (Thermo Fisher Scientific). Mobile phase A consisted of 0.1% (v/v) formic acid and mobile phase B of 80% (v/v) acetonitrile with 0.1% (v/v) formic acid. Flow-rate of 0.3 μL/min using gradients optimized for each chromatographic fraction from offline fractionation ranging from 2% mobile phase B to 45% mobile phase B over 90 min. The MS data was acquired in data-dependent mode using the top-speed setting with a three second cycle time. For every cycle, the full scan mass spectrum was recorded in the Orbitrap at a resolution of 120,000 in the range of 400 to 1,600 m/z. Ions with a precursor charge state between 3+ and 6+ were isolated and fragmented. Fragmentation by Higher-energy collisional dissociation (HCD) employed a decision tree logic with optimized collision energies (Kolbowski et al., 2017). The fragmentation spectra were then recorded in the Orbitrap with a resolution of 30,000. Dynamic exclusion was enabled with single repeat count and 60 s exclusion duration.

A recalibration of the precursor m/z was conducted based on high-confidence (< 1% false discovery rate (FDR)) linear peptide identifications (Lenz et al., 2018). The recalibrated peak lists were searched against the sequences and the reversed sequences (as decoys) of crosslinked peptides using the Xi software suite (v.1.6.745) for identification (Mendes et al., 2019). The following parameters were applied for the search: MS1 accuracy = 3 ppm; MS2 accuracy = 10 ppm; enzyme = trypsin (with full tryptic specificity) allowing up to three missed cleavages; crosslinker = BS3 with an assumed reaction specificity for lysine, serine, threonine, tyrosine and protein N termini; fixed modifications = carbamidomethylation on cysteine; variable modifications = oxidation on methionine, hydrolyzed/aminolyzed BS3 from reaction with ammonia or water on a free crosslinker end. The identified candidates were filtered to 2% FDR on link level using XiFDR v.1.1.26.58 (Fischer and Rappsilber, 2017). See Table S2 for further characterization of Smc5/6 crosslinking analysis.

In vitro Smc5/6 loading assay

For topological loading assays, 165nM of Smc5/6 complex was mixed with 3.3 nM DNA in a reaction volume of 15 μL and incubated on ince in 56L buffer (40 mM Tris-HCl pH 7.5, 3 mM DTT, 7 mM MgCl2, 50 mM NaCl, 15% glycerol, 0.003% Tween) with or without 2 mM ATP. After 5min, samples were incubated for further 35min at 30°C with gentle agitation (400rpm) using a thermos-shaker. The loading reaction was stopped by the addition of 500 μL of 56S buffer (40 mM Tris-HCl pH 7.5, 1 mM DTT, 500 mM NaCl, 10 mM EDTA, 5% glycerol, 0.35% Triton X-100) and incubation for 5min at 30°C, followed by 5 min on ice. Smc5/6-DNA complexes were immunoprecipitated using a μMACS HA isolation kit (Miltenyi Biotec). 20 μL of magnetic beads were added to each reaction and rocked at 4 °C for 45 min. The magnetic beads were washed three times with 400 μL of 56W1 buffer (40 mM Tris-HCl pH 7.5, 1 mM DTT, 750 mM NaCl, 10 mM EDTA, 0.35% Triton X-100) and then once with 400 μL of 56W2 buffer (40 mM Tris-HCl pH 7.5, 1 mM DTT, 200 mM NaCl, 0.1% Triton X-100). Beads were then suspended in 15 μL elution buffer (10 mM Tris/HCl, pH 7.5, 1 mM EDTA, 50 mM NaCl, 0.75% SDS, 1 mg ml^{-1} protease K) and incubated at 50 °C for 20 min. For assays involving linearization PstI digestion at 4 °C for 120 min was used. The reactions were resolved by electrophoresis for 1 h at 80V on 0.8% (w/v) TAE-agarose gels at 4°C. DNA was either detected on a fluorescent image analyzer FLA-5000 (Fujifilm) after SYBR Green I (Invitrogen, ThermoFisher Scientific) gel staining or using ethidium bromide staining and UV. Band intensities quantified using ImageQuant.

For Figure 4B, pUC19 was used as DNA substrate. Relaxed, supercoiled, positively supercoiled pBR322 and *Crithidia fasciculata* kDNA used in Figures 4C and 4D were obtained from Inspiralis.

Magnetic tweezers DNA substrate

DNA substrate for magnetic tweezers experiments consisted of a 6337 bp-central fragment produced from the pNLrep plasmid by digesting with KpnI and PsiI enzymes (both from NEB) and two digoxigenin or biotin-labeled DNA handles. Handles were PCR-generated from the plasmid pSP73-JY0 (Fili et al., 2010) using oligos (forward: 5′-GCGTAAGTGGTACCTTATAAAGTACTCGACT-CACTATAGGGAGACCGGC; and reverse: 5′-AGTAAGCGCCGTCAGACCAG), incorporating Dig-dUTP or Bio-dUTP (Roche). Dig- and Bio-handles were digested with KpnI or PsiI, respectively, and ligated with the central fragment using T4 DNA ligase (NEB). This procedure allowed us to obtain a high yield of torsionally-constrained as well as some residual nicked DNA molecules for MT experiments. We avoided the exposure of the DNA to intercalating agents as well as to UV light during the production of all DNA substrates.

Magnetic tweezers assays

We employed a custom-built MT setup similar to the system described previously (Seidel et al., 2004; Strick et al., 1998). In our assays, a DNA construct (6.3 kbp) is tethered between a glass slide covered with anti-digoxigenin and 1-μm streptavidin-coated superparamagnetic beads (Dynabeads MyOne Streptavidin, Thermo Fisher). A couple of permanent magnets that can be translated along the optical axis of the microscope or rotated are used to stretch and twist the DNA. The magnetic beads are visualized using an inverted optical microscope while the bead position (DNA extension) is measured in real-time by video-microscopy, allowing us to monitor the dynamics of DNA modifying complexes at the single-molecule level. The full system is controlled by an in-house LabVIEW software allowing real-time measurements of tens of beads at 120 Hz. The force is calculated from the Brownian excursions of the bead in Fourier space and corrected for low pass filtering and aliasing (Daldrop et al., 2015).

Single nicked, single torsionally constrained and double DNA tethers were identified prior to each experiment by performing extension versus magnet turns curves at high and low forces. Single nicked DNA molecules show no change in extension with rotations. Single torsionally constrained DNA molecules do not display plectonemes at negative turns at high force but do form plectonemes at low force. So, their mechanical response differs from that of double tethers, whose extension decreases both with positive and negative turns, as the DNA molecules entangled. All the experiments were done at room temperature in a buffer containing 50 mM NaCl, 40 mM Tris-HCl, pH 7.5, 7 mM $MgCl_2$, 3 mM DTT, supplemented with 50 μM biotin when flowing the Smc5/6 complex, unless stated otherwise. Additionally, DNA-bound streptavidin-covered magnetic beads were incubated with 450 μM biotin prior to their introduction in the fluidics cell, to minimize possible unspecific interactions with the StrepII-tag of the complex. The samples with Smc5/6 were injected into the fluidics cell at 20 μl/min. Shown traces include raw data (120 Hz) and a 3 Hz filtering.

ctN4 *in vitro* SUMOylation reaction

For SUMOylation of ctN4 (C-terminal fragment of Nse4, residues 246 to 402), 2 μM ctN4 was added to SUMOylation reactions in the same conditions as described above. The products were analyzed by SDS-PAGE followed by Oriole staining.

Liquid chromatography-tandem mass spectrometry (LC-MS/MS)

Samples were processed by in-Stage Tip (iST) digestion (Preomics GmbH, Planegg/Martinsried) following the manufacturer recommendation. Protein digests were solubilised in 30 μL of reconstitution buffer and were transferred to auto sampler vials for LC-MS analysis. Peptides were separated using an Ultimate 3000 RSLC nano liquid chromatography system (Thermo Scientific) coupled to an LTQ Orbitrap Velos mass spectrometer (Thermo Scientific) via an EASY-Spray source. Sample volumes were loaded onto a trap column (Acclaim PepMap 100 C18, 100 μm x 2 cm) at 8 μl/min in 2% acetonitrile, 0.1% TFA. Peptides were eluted on-line to an analytical column (EASY-Spray PepMap C18, 75 μm x 50 cm). Peptides were separated using a ramped 120 min gradient

from 1%–42% buffer B (buffer A: 5% DMSO, 0.1% formic acid; buffer B: 75% acetonitrile, 0.1% formic acid, 5% DMSO). Eluted peptides were analyzed operating in positive polarity using a data-dependent acquisition mode. Ions for fragmentation were determined from an initial MS1 survey scan at 30,000 resolution (at m/z 200) in the Orbitrap followed by CID (Collision-Induced Dissociation) of the top 10 most abundant ions in the Ion Trap. MS1 and MS2 scan AGC targets set to 1e6 and 1e5 for a maximum injection time of 50 ms and 110 ms, respectively. A survey scan m/z range of 350 – 1500 m/z was used, with CID parameters of isolation width 1.0 m/z, normalized collision energy of 35%, activation Q 0.25 and activation time of 10ms.

Data were processed using the MaxQuant software platform (v1.6.2.3) with database searches carried out by the in-built Andromeda search engine against the Uniprot *Saccharomyces cerevisiae* database (6,729 entries, v.20180305). A reverse decoy database was created and results displayed at a 1% false-discovery rate (FDR) for peptide spectrum matches and protein identification. Search parameters included: trypsin, two missed cleavages, fixed modification of cysteine carbamidomethylation and variable modifications of methionine oxidation, asparagine deamidation and protein N-terminal acetylation. Label-free quantification was enabled with an LFQ minimum ratio count of 2. 'Match between runs' function was used with match and alignment time limits of 0.7 and 20 min, respectively. Protein and peptide identification and relative quantification outputs from MaxQuant were further processed in Microsoft Excel, with hits to the 'reverse database', 'potential contaminants' (peptide list only) and 'Only identified by site' fields removed.

Electrophoretic gel mobility shift assay

6-carboxyfluorescein (6-FAM) 45nt-ssDNA and dsDNA substrates were prepared as described before (Terakawa et al., 2017). 50 mM of ssDNA or dsDNA were incubated with increasing concentrations of Smc5/6 complex ranging from 100 to 400 nM for 30 min at 28°C in 40 mM Tris–HCl pH 7.5, 50 mM NaCl, 7mM $MgCl_2$, 10% glycerol, 0.2% NP-40 and 5 mM BME in a final volume of 15 μl in the presence or absence of 8 mM ATP. The reactions were resolved by electrophoresis for 16 h at 30 V on 0.4% (w/v) 0.5xTAE-agarose gels at 4°C. DNA was detected on a fluorescent image analyzer FLA-5000 (Fujifilm) after SYBR Safe (Invitrogen, ThermoFisher Scientific) gel staining.

QUANTIFICATION AND STATISTICAL ANALYSIS

ATPase assays

ATPase assay data in Figure 1C are shown as the mean ± SD. Three independent experiments were performed (n = 3).

SUMOylation assays

In vitro SUMOylation assays in Figures 1E and 1F depict the mean (red lines) and standard deviation (black lines) values. Three independent experiments were performed (n = 3).

DNA topological binding

In vitro topological binding assays shown in Figure 4D depict the mean (orange lines) and standard deviation (black lines) values. Three independent experiments were performed (n = 3).

Magnetic tweezers experiments

Regarding the quantification of compaction described in Figure 5D, bars represents mean ± SE. The number of DNA molecules is indicated in the main text.

Regarding the quantification of condensed extension after rotations in Figure 6E, boxplots indicate the median, 25th and 75th percentiles of the distributions and the whiskers show the outlier. The sample number varies between $48 \leq n \leq 119$. (Nicked +10 turns, n = 101; TC +10 turns, n = 76; Double +10 turns, n = 59; Nicked −10 turns, n = 119; TC −10 turns, n = 108; Double −10 turns, n = 48). Statistical analysis and data representation was performed using OriginPro 8.